NJC

New Journal of Chemistry

An international journal of the chemical sciences

www.rsc.org/njc

Volume 34 | Number 7 | July 2010 | Pages 1225–1492

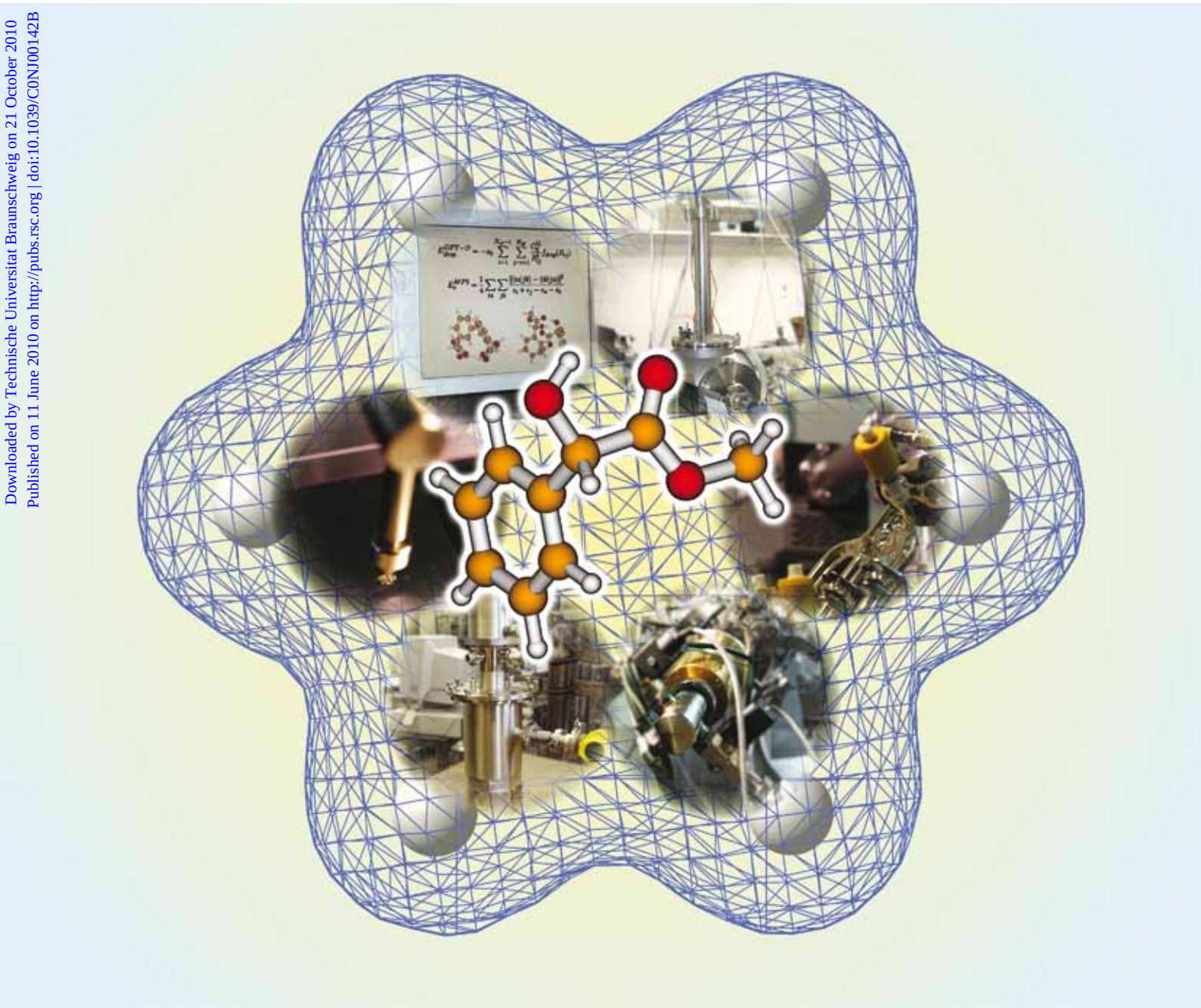

ISSN 1144-0546

RSC Publishing

PAPER

Martin A. Suhm and
Anne Zehnacker-Rentien *et al.*
Chirality influence on the aggregation
of methyl mandelate

Chirality influence on the aggregation of methyl mandelate†

Merwe Albrecht,[a] Ana Borba,[b] Katia Le Barbu-Debus,[c] Birger Dittrich,[d] Rui Fausto,[b] Stefan Grimme,[e] Ahmed Mahjoub,[c] Marija Nedić,[a] Ulrich Schmitt,[a] Lena Schrader,[a] Martin A. Suhm,*[a] Anne Zehnacker-Rentien*[c] and Julia Zischang[a]

Received (in Montpellier, France) 22nd February 2010, Accepted 19th April 2010
First published as an Advance Article on the web 11th June 2010
DOI: 10.1039/c0nj00142b

The methyl ester of mandelic acid is investigated by a wide range of techniques to unravel its aggregation pattern and the influence of relative chirality of the aggregating monomers. Matrix isolation confirms that a single monomer conformation prevails. The electronic spectrum of the dimers is strongly affected by the relative monomer chirality. Vibrational effects are more subtle and can be explained in terms of the most stable homo- and heteroconfigurational dimer structures, when compared to results of MP2 and DFT-D computations. Selective IR/UV double resonance techniques and wide-band FTIR spectroscopy provide largely consistent spectroscopic fingerprints of the chirality discrimination phenomena. The dominant homochiral dimer has two intermolecular O–H···O=C hydrogen bonds whereas the more strongly bound heterochiral dimer involves only one such hydrogen bond. This is a consequence of the competition between dispersion and intramolecular or intermolecular hydrogen bonding. Aromatic interactions also play a role in trimers and larger clusters, favoring homochiral ring arrangements. Analogies and differences to the well-investigated methyl lactate system are highlighted. Bulk phases show a competition between different hydrogen bond patterns. The enantiopure, racemic, and 3 : 1 crystals involve infinite hydrogen-bonded chains with different arrangements of the aromatic groups. They exhibit significantly different volatility, the enantiopure compound being more volatile than the racemic crystal. The accumulated experimental and quantum-chemical evidence turns methyl mandelate into a model system for the role of competition between dispersion forces and hydrogen bond interactions in chirality discrimination.

1 Introduction

Most molecules of biological interest are chiral and their mutual interaction depends, in a more or less pronounced way, on this lack of mirror symmetry. Although these effects of intermolecular diastereoisomerism tend to become more prominent with an increasing number of chiral centers, they may be characterized in more detail for small aggregates of simple prototype molecules, embedded in an inert environment or even better in no environment at all. This calls for gas phase studies,[1] which need to be carried out at low temperatures (in supersonic jets) in order to stabilize pairs or larger assemblies of molecules. Once established, these cluster studies may be related to properties of bulk matter, such as chirality dependent vapor pressures,[2] polymorphism,[3,4] enantio-enriched crystallization[5] or even reactivity.[6]

Among the most pronounced chirality recognition phenomena observed in the gas phase, the protonated serine octamer case stands out and has even been discussed in the context of the homochirality of life.[7] It lends itself well to mass spectrometry studies, which offer unsurpassed size selectivity and sensitivity.[8,9] For neutral complexes, a somewhat different experimental repertoire is available.[1] Fourier transform infrared (FTIR) spectroscopy is universally applicable, covers a wide spectral range and has revealed a chirality-dependent hydrogen bond topology switch in methyl lactate tetramers,[10,11] by comparing spectra of enantiopure and racemic samples. Because this technique lacks rigorous size selection, complementary investigations using crossed molecular beam techniques can be helpful.[12] Previous to that work, dramatic chirality recognition effects in dimers were identified by IR/UV double resonance techniques,[13–16] which are more sensitive and isomer- as well as mass-selective, but require a suitable UV chromophore in the molecule and involve chirality-dependent properties of the electronically excited state.

[a] *Institut für Physikalische Chemie, Universität Göttingen, D-37077 Göttingen, Germany. E-mail: msuhm@gwdg.de*
[b] *Department of Chemistry, University of Coimbra, P-3004-535 Coimbra, Portugal*
[c] *CNRS, Institut des Sciences Moléculaires d'Orsay, FRE3363, Univ. Paris-Sud Orsay, F-91405, France. E-mail: anne.zehnacker-rentien@u-psud.fr*
[d] *Institut für Anorganische Chemie, Universität Göttingen, D-37077 Göttingen, Germany*
[e] *Organisch-Chemisches Institut (Theoretische Chemie), Universität Münster, D-48149 Münster, Germany*

† Electronic supplementary information (ESI) available. CCDC reference numbers 762619–762621.

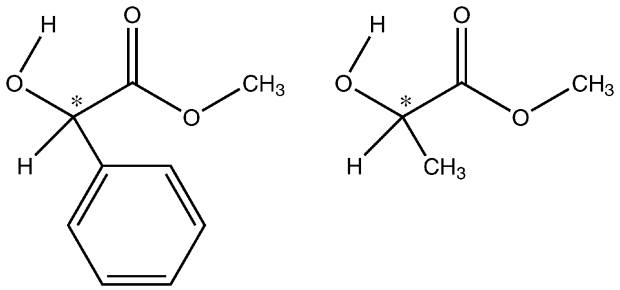

A combination of FTIR and IR/UV techniques for the same system would be most desirable and could provide a comprehensive picture of the chirality recognition process in a supersonic expansion. Until recently,[17] such a combination was limited by the lack of heatable nozzles in the jet-FTIR approach. Now, it is possible to study compounds which have a vapor pressure of less than 1 mbar at 450 K. Therefore, it appeared timely to study methyl mandelate (MM), the methyl/phenyl-substituted analog of methyl lactate, by such a combination of different approaches.

The methyl ester of mandelic acid combines a number of features which makes it particularly interesting for an aggregation study. Being a chiral α-hydroxyester, it offers a close competition between strained intramolecular OH···O=C hydrogen bonding and a range of intermolecular hydrogen bond options. The latter may be of the isolated OH···O=C type, of cooperative OH···OH···O=C nature, of the bifurcated type or else they may involve cyclic, mutually reinforcing OH···OH···OH contacts, complemented by somewhat weaker interactions involving the ester oxygen or the α-CH. Peculiar to racemic methyl lactate tetramer is the outperformance of the isolated OH···O=C hydrogen bond pattern over the cyclic OH arrangement, if the four molecules are combined in a singular chirality sequence. If only one of the monomers exhibits the wrong handedness, the isolated pattern appears to lose its particular energy advantage.[10]

By switching from methyl lactate to methyl mandelate, an important interaction site is added, because the π electron clouds of the phenyl rings may undergo stacking and X–H···π interactions.[18,19] These may compete with or add to the hydrogen bond contacts. Furthermore, the phenyl substituent has an effect on the strength of the intramolecular hydrogen bond in the monomer, shortening it by about 1% and softening the OH oscillator by about 1%. Thus, the mandelate system offers exciting new tuning parameters to the α-hydroxy ester class of compounds, in addition to its accessibility to a wider range of experimental techniques.

Beyond their relevance from a model building perspective, mandelates and in particular the free mandelic acid also find practical applications in the field of enantioselective chemistry, notably in the separation of racemates,[3,20] with important applications in the pharmaceutical industry.

Methyl mandelate has been investigated before in its monomeric form by vibrational spectroscopy in CCl_4 solutions[21–23] and with IR/UV spectroscopy.[24] Spectra and conformational preferences as a function of aggregation state are still missing, in contrast to the extensive studies of methyl lactate, both experimental and theoretical.[10–12,16,25–30] A recent study of the mixed methyl lactate/methyl mandelate dimer[24] was interpreted in terms of an unusual conformational preference of the lactate unit. The purely aromatic system allows for a better understanding of the role of London dispersion effects in non-covalent interactions.

In the present work, the aggregation behavior of methyl mandelate was therefore studied by various spectroscopic techniques, namely jet-FTIR, matrix-FTIR and ionization-detected IR/UV double resonance spectroscopy. In the electronic and vibrational spectra of the jet-cooled aggregates, characteristic differences between the enantiopure and racemic samples, and both similarities as well as differences between mandelates and lactates were found. The focus of the present experimental and computational analysis lies on the dimers of methyl mandelate, but larger clusters are also observed similar to those of methyl lactate.[10,11]

Complementary to the experimental jet data on the smallest aggregation units, a wide range of matrix isolation, amorphous and crystalline solid, enantiopure, racemic, and 3 : 1 crystal structure, vapor pressure and quantum chemical studies of methyl mandelate were added to provide a compelling collection of information on chirality-dependent effects in this model system. Matrix isolation is particularly powerful in detecting or excluding minor contributions of less stable monomer conformations.[26] Spectra of glass-like bulk compounds can indicate metastable hydrogen bond patterns, which may then be converted to stable ones upon annealing.[31] Structural information from X-ray crystallography of single crystals with different enantiomeric composition provides a detailed picture of the infinite aggregation limits. Solid state vapor pressure differences[2] reflect enantioselective differences in the hydrogen bond and the van der Waals network of the solid.

To assign the observed bands in the vibrational spectra and to obtain further insights into the chirality-dependent aggregation behavior, quantum chemical calculations are essential[32] and were carried out in the present study using different approaches. For an overview of the hydrogen bonded dimers, density-functional theory (DFT) calculations were performed, but geometry optimization at small basis set MP2 level shows that dispersion interactions play an essential role in the aggregation of methyl mandelate. To carry these effects over into vibrational spectra, dispersion-corrected DFT calculations using our standard technique (termed DFT-D) were performed.[33–35] Particular emphasis is put on hydrogen bond-induced vibrational OH-stretching shifts. Such shifts are typically bathochromic and we use the colloquial term "red shift", which would be more appropriate in the visible range. "Blue shifts" may also occur in this particular system, because of the competition between intramolecular and intermolecular hydrogen bonds. This competition opens the arena for chirality control *via* aromatic contacts.

2 Methods

S-Methyl mandelate (*S*-MM) (99% ABCR, 98% Alfa Aesar, or ≥ 99% Sigma Aldrich) and racemic methyl mandelate (MM) (97% Alfa Aesar or ≥ 98% Fluka) were used without further purification for the jet-FTIR and matrix experiments. Different suppliers were explored to exclude the influence of

impurities on the spectra, in particular for the racemic mixture. For the IR/UV experiments *S*-MM, *R*-MM and racemic MM ($\geq$ 99% Sigma Aldrich) were used as provided. The experimental setups are only described briefly and references are given for further details.

2.1 Matrix isolation and solid films

Matrix isolation spectra were obtained by co-deposition of the isolating gas (argon, 99.9999% Air Liquide) and the compound on to the cooled (10 K) CsI substrate connected to the cryostat (APD Cryogenics closed cycle helium refrigeration system with a DE-202A expander). A glass vacuum system and standard manometric procedures were used to deposit the isolating gas. MM was placed in a specially designed, doubly thermostated Knudsen cell with shut-off possibility whose main component is a NUPRO (SS 4BMRG) needle valve.[36] The temperature of the valve and of the sample compartment was kept at room temperature in most experiments. Solid films of the neat compounds were prepared in a way similar to that used to obtain the matrices, but in this case only vapors of the compounds were deposited onto the CsI substrate of the cryostat. In the annealing experiments, the temperature was controlled and measured by a diode temperature sensor connected to a Scientific Instruments digital temperature controller (model 9659) to within 1 K. The temperature variation during the annealing was done in steps of 5 K in the matrix isolation experiments and 10–20 K in the studies on the neat solids. The IR spectra were collected at 0.5 cm^{-1} spectral resolution on a Nicolet 6700 Fourier transform infrared spectrometer, equipped with a deuterated triglycine sulfate (DTGS) detector and a Ge/KBr beam splitter. To accommodate the cryostat head and to allow for efficient purging of the instrument by a stream of gas to remove water and CO_2 vapors, modifications of the sample compartment of the spectrometer were made.[37]

2.2 ATR spectra

A single reflection ZnSe attenuated total reflection (ATR) unit was used to obtain solid state mid IR spectra of finely ground MM crystals. In comparison to KBr pellet spectra, the ATR spectra showed a better peak resolution, but also some scattering effects at high wavenumber. Only spectral regions with significant differences between enantiopure and racemic samples were considered. This significance was further corroborated by studying powders which were pre-treated by melting or by methanol dissolution.

As chirality recognition effects in crystals are expected to be most pronounced in the far infrared, we have also employed a diamond ATR unit (Harrick, MVP-Pro-Star) coupled to a He-cooled Si bolometer in a Bruker Vertex 70 v spectrometer equipped with a massive silicon beam splitter to compare the spectra of different crystals between 30 and 470 cm^{-1}.

2.3 X-ray structures

All data sets were collected on a Bruker SMART 6000 system equipped with a copper rotating anode at a temperature of 100 K. Data collection and reduction was performed with the programs APEX2 and SAINT 7.61A, scaling and the empirical absorption correction with SADABS.[38] For structure solution and initial independent-atom model (IAM) refinements SHELX[39] was used. To gain more confidence in the assignment of absolute structure and the configuration of chiral carbon atoms an invariom refinement[40] was carried out with the full-matrix least squares refinement program XDLSM.[41] In such a refinement, theoretically predicted non-spherical scattering factors of the Hansen & Coppens multipole model[42] as stored in the invariom database[43] are used that lead to an improved fit to the observed data and hence to smaller standard deviations for all parameters including the Flack[44] parameter when compared to the IAM result. More recent work[45] has shown that the probability of a wrong assignment can also be ruled out based on statistical methodology even if the standard deviation of the Flack parameter does not indicate strong inversion-distinguishing power.[46]

2.4 Jet FTIR spectra

For the jet FTIR measurements a heated single or double 10×0.5 mm^2 slit nozzle was used to generate the clusters of methyl mandelate. Descriptions of the experimental setup (popcorn jet) may be found elsewhere.[17,47] In short, gas pulses of 0.3 s duration emerging from the nozzle were synchronized to FTIR scans (Bruker IFS 66v) and the signal was detected by an InSb or HgCdTe detector after optical filtering of unwanted spectral ranges. The intense gas pulses (He with a trace of the desired compound) were diluted in a large vacuum chamber before being pumped away. The gas mixture was prepared by flowing the He through a heated sample container enclosed between two check valves. As the melting point of enantiopure *S*-methyl mandelate is only 328–329 K[48] and that of racemic methyl mandelate only 325–327 K,[49] the substance was adsorbed on a dried molecular sieve, to keep a large surface area while heating the sample container above the melting point.

2.5 Jet R2PI and IR/UV experiments

The experimental setup has been described previously[50] and consists of a pinhole nozzle combined with ion detection. The methyl mandelate sample, heated at 413 K to increase its vapor pressure, was seeded in neon at a pressure of $\approx$1 bar and expanded into vacuum through a 300 μm pulsed nozzle (General Valve). The resulting supersonic beam was intersected by two laser beams in the ion-source region of a linear time-of-flight mass spectrometer (R. M. Jordan). The ions were detected by a microchannel plate detector (R. M. Jordan, 2.5 cm) mounted on top of a 1 m flight tube. The ion signal was averaged by an oscilloscope (Lecroy wavesurfer) and processed through a PC.

Mass-resolved electronic S_0–S_1 spectra were recorded by employing one-colour-resonant two-photon ionization (R2PI).

Mass-resolved vibrational spectra were obtained using resonant ion dip infra-red (RIDIR) spectroscopy. Briefly, the UV probe laser was tuned on an electronic transition of the selected species and induced an ion current which was a measure of the population of the probed species. The wavelength of the IR pump laser was scanned in the region of interest.

When it came into resonance with a vibrational transition, the resulting depletion of the probed species manifested itself as a dip in the ion signal.

The tunable UV laser source was obtained by mixing a frequency-doubled dye laser (Quantel TDL90 equipped with LDS 722 dye) with the fundamental radiation of the same YAG laser (Quantel). The tunable IR source was a Euroscan OPO based on a KTP crystal. Electronic spectra were recorded without focusing the UV beam. For double resonance spectra, the two beams were co-focused with a 500 mm focal length lens onto the cold region of the jet. The IR pulse was set 100 ns before the UV pulse; the spectral resolution of the UV was 0.2 cm^{-1} and that of the IR 2 cm^{-1}. The time duration of the pulses was 10 ns.

2.6 Mass spectra

Relative vapor pressures have been determined using a quadrupole mass spectrometer (Stanford Research Systems RGA 200). Its vacuum chamber was pumped by a small turbomolecular pump (Leybold Turbovac 50) backed by a rotary vane pump (Vacuubrand RS-4) with a cold trap. Liquid samples, degassed by several freeze-pump-thaw cycles, or solid samples were thermostatted in a bath cryostat (Haake CH/F3). The vapor was introduced into the mass spectrometer through a high precision needle valve (HOKE Milli-Mite). For a certain setting of the valve a stable dynamical equilibrium of leakage into the chamber and pumping-off was obtained after an induction period of a few minutes.

The currents of characteristic fragment ions obtained at an electron energy of 70 eV and measured with a Faraday cup detector were taken as a measure of relative vapor pressure of the parent compound in the sample. The method has been tested and verified in a series of measurements on *n*-alkanols of low vapor pressure[51] and mixtures thereof (*e.g.*, 1-octanol and 1-decanol[52]).

2.7 Quantum chemical calculations

Quantum chemical calculations at the B3LYP and MP2 levels with the standard 6-31+G* and 6-31G** basis sets were performed using the Gaussian 03 program suite.[53] At the MP2 level, these basis sets must be considered rather small, but larger basis set calculations for methyl mandelate dimers would be quite demanding. To alleviate this limitation dispersion-corrected density functional theory (DFT-D[54]) calculations at the RI-B97-D/def2-TZVP[54–56] level were performed using the Turbomole 5.9 program system.[57]

The following procedure has been used to explore the potential energy surface in all its conformational wealth. First, a model potential energy surface built on a semi-empirical potential[58] has been explored by simulated annealing. As this model potential keeps all the intramolecular coordinates frozen, other relevant structures involving opening of the intramolecular hydrogen bond have been created, guided by chemical intuition. The set of complexes defined above has been used as starting points for a full optimization at the B3LYP level. The more relevant structures have been further optimized at the MP2 or DFT-D levels. As the size of the system rules out the canonical MP2 level for the harmonic frequencies calculations, they have been calculated at the DFT-D level as numerical derivatives of analytic first derivatives using the program SNF.[59]

When comparing experimental dimer bands of methyl mandelate with theoretical predictions in figures, all calculated wavenumbers are multiplied by a scaling factor to match the experimental monomer transitions. The scaling factor differs between the OH and C=O stretching region. In this way, electronic structure deficiencies and anharmonic contributions to the fundamental vibrations are corrected to first order. A graphical comparison of dimer band positions is thus more straightforward. In contrast, tabulated wavenumbers are always unscaled.

3 Results and discussion

3.1 Matrix isolation

Matrix isolation spectra were recorded to find out if methyl mandelate exists in different monomer conformations as in the case of the related methyl lactate.[26] The matrix spectrum of methyl mandelate in an argon matrix after deposition at 10 K shows a broadly structured band in the OH stretching region due to site splittings (Fig. 1). Upon annealing up to 40 K, relaxation of the molecules into the most stable site is observed and only one band at 3520 cm^{-1} survives at 40 K. A very weak band at 3612 cm^{-1} indicates trace contributions of a second conformation, which could not be further quantified due to the onset of aggregation.

In the carbonyl region only one strong band with weak annealing dependence is observed at 1744 cm^{-1}. A very weak satellite band near 1764 cm^{-1} again indicates trace amounts of a second isomer. By comparison with the calculated spectra for the two most stable conformers of monomeric isolated methyl mandelate (Fig. 7 in section 3.3), the presence of more than 3% of this second conformer can be ruled out.

In other spectral ranges (Fig. 1, top part), there is also no evidence for significant amounts of a second conformer. Upon annealing of the matrix beyond 40 K, aggregation sets in. The spectral changes are characteristic for stronger hydrogen bond formation, with red shifts in the OH and C=O stretching fundamentals as well as partial blue shifts in the bending range. The aggregation remains spectrally broad until the matrix starts to evaporate near 45 K.

The matrix isolation results are in good agreement with higher temperature solution studies.[21–23] The latter had revealed an internally C=O hydrogen bonded OH stretching fundamental near 3536–3551 cm^{-1}, together with a much weaker feature near 3603–3613 cm^{-1}, which was tentatively attributed to a weaker OH hydrogen bond, either to the phenyl ring or to the ester OCH_3 group. The C=O stretching fundamental was located near 1737–1739 cm^{-1}, and its weak overtone assigned at 3455 cm^{-1}, about 0.5% below the harmonic prediction.[22] It is not detected in the matrix isolation spectra.

For the following supersonic jet work, one may thus safely assume the presence of a single monomer conformation, which profits from a strong intramolecular hydrogen bond.

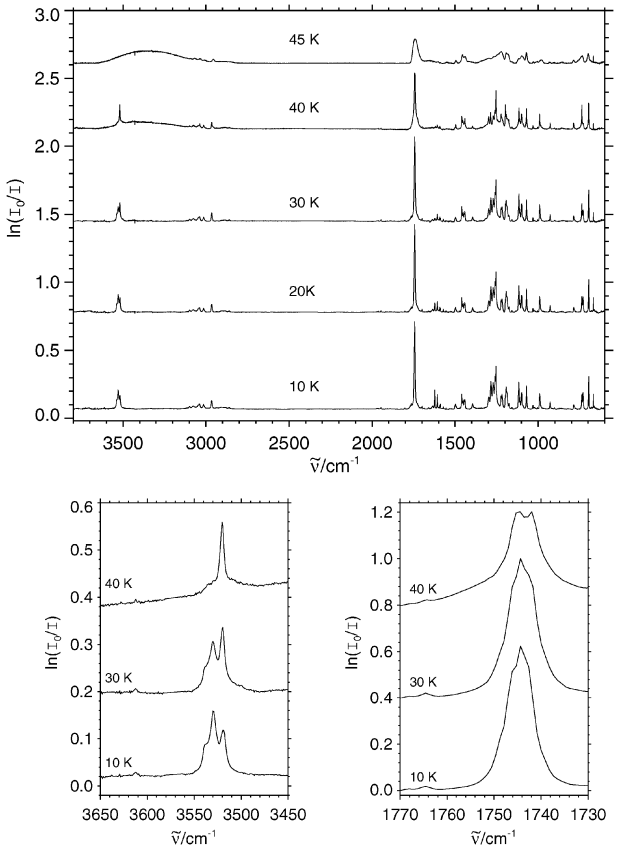

Fig. 1 Infrared spectra of methyl mandelate in an argon matrix at different temperatures during an annealing experiment. The bottom part shows enlarged O–H and carbonyl stretching regions.

3.2 Supersonic jet spectra

3.2.1 FTIR spectroscopy. The jet-cooled FTIR spectra show only one monomer band in the OH stretching region at 3549 cm^{-1}. It may be compared to the corresponding IR/UV double resonance peak, which was recently reported at 3565 cm^{-1}.[24] In the present work, it was re-determined at 3552 cm^{-1} using the same technique. This is in better agreement with the calibrated FTIR value. The resulting Ar matrix shift of ≈ -30 cm^{-1} for the most stable matrix site (see the preceding section) is fairly large, but consistent with the observed extensive site splittings in the matrix (Fig. 1). Clearly, the intramolecular hydrogen bond reacts sensitively to the detailed position of the neighboring Ar atoms. The matrix shift of the carbonyl fundamental is much smaller, namely -8 cm^{-1} (Table 1).

An advantage of jet-cooling over matrix isolation is that aggregation can often be controlled in such a way that spectrally separated dimers and oligomers may be assigned. This is exemplified in Fig. 2, which shows spectra of both racemic and enantiopure MM expansions in helium under nominally identical conditions, together with the difference between the two. Slight differences in sample preparation on the molecular sieve are unavoidable, but the conditions are seen to be remarkably similar, in particular when comparing the CH stretching fundamentals near 3000 cm^{-1}. A slightly higher signal in the enantiopure expansion may be due to differences in vapor pressure (see section 3.6), but it is largely masked by other variations.

Table 1 Experimental band positions $\tilde{\nu}$(O–H)/cm^{-1} and differences between aggregate (A = D,T,C) and monomer (M) bands $\Delta\tilde{\nu}_{(A-M)}$/$cm^{-1}$, revealing predominantly homochiral (hom) and heterochiral (het) cluster contributions

	Jet FTIR		IR/UV		Jet FTIR	
	$\tilde{\nu}$(O–H)	$\Delta\tilde{\nu}_{(A-M)}$	$\tilde{\nu}$(O–H)	$\Delta\tilde{\nu}_{(A-M)}$	$\tilde{\nu}$(C=O)	$\Delta\tilde{\nu}_{(A-M)}$
M	3549	—	3552	—	1752	—
D-hom	3539	−10	3541	−11	1753	+1
D-hom	3521	−28	3522	−30	1763	+11
D-het	3556	+7	3559	+7	1735	−17
D-het	3514	−35	3518	−34	1760	+8
D-het	3533	−16	3532	−20	—	—
T-hom	3461	−88	—	—	—	—
C-hom	3301	−248	—	—	—	—

Apart from such subtle intensity issues, the monomer OH stretching fundamental (marked M) must be identical for both expansions, but there are major differences in several other spectral features. These are clearly due to chirality recognition phenomena,[1] namely different vibrational frequencies in diastereomeric clusters of MM. The clusters in Fig. 2 are differentiated between dimers (D), trimers (T) and cyclic tetramers and larger clusters (C). In some cases, only the intensity is affected, such as in the first band to the right (red) of the monomer OH signal. Being about twice as strong in the enantiopure expansion, it is obviously due to a homoconfigurational dimer, which is statistically 50% less abundant in a racemic expansion. Other weakly shifted bands and shoulders only appear in the racemic expansion and are thus specifically due to heteroconfigurational dimers. Further shifted into the red region, where one expects larger clusters such as trimers and tetramers, the differences are also quite pronounced. The enantiopure expansion appears to have a

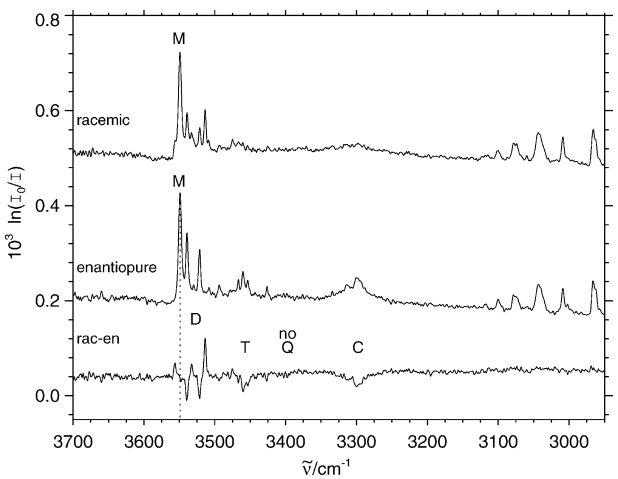

Fig. 2 Jet FTIR spectra of the racemate (T_{sample} = 363–373 K, 2000 co-added spectra) and the *S* enantiomer (T_{sample} = 363–373 K, 1800 co-added spectra) of methyl mandelate and the difference of the two spectra with the bands of the heterochiral clusters (D, residual T and C, no Q) pointing upwards and the bands of the homochiral clusters (D, T, C) pointing downwards. Monomer (M) contributions cancel perfectly, if the racemic spectrum is multiplied by 1.03 before subtraction of the enantiopure spectrum.

stronger clustering propensity, given the stronger signals. The bands are also sharper, indicative of a larger structural homogeneity of the underlying clusters. This is qualitatively reminiscent of the methyl lactate case,[10] but a feature corresponding to the "magic" C═O···HO connected heterochiral tetramer (Q) appears to be missing. Instead, the band positions and widths are more consistent with cooperative cyclic OH···OH···OH hydrogen bond motifs.[10] In such cycles, homochirality offers the advantage that all aromatic rings are on the same side and can interact *via* dispersion interactions. This could explain the stronger clustering propensity.

However, this analysis must remain qualitative at this stage and the focus of the present spectroscopic study is on dimers. These dimer features are particularly easy to classify in the difference spectrum (lowest trace), because their distribution among homo- and heterochiral pairings is rather symmetric implying not too different IR band strengths. The three positive signals in the difference spectrum are due to heteroconfigurational dimers. It has been carefully checked by sample purity variations that the two weakest bands are not due to impurities. Their intensity may be distorted by the nearby monomer subtraction, but we clearly attribute them to MM clusters. This is also true for the strongest heterochiral band, which is found at a lower wavenumber. The two narrow negative signals in the difference spectrum are due to homoconfigurational dimers, which are statistically depleted in the racemic expansion. They occur at a lower wavenumber than the monomer.

The cancellation of the monomer signal in the difference spectrum works quite well in this case despite slight particle scattering artifacts in the spectra (dispersion-like band shape contributions[17]), but IR/UV double resonance techniques can provide a more elegant separation of the dimers from the monomer signals. The reason is that the double resonance technique allows the spectra of the monomer or the heterochiral and homochiral dimers to be recorded separately, provided that they show specific electronic spectra.

3.2.2 Electronic spectroscopy. The monomers and dimers have very different electronic spectra, which are shown in Fig. 3. The monomer shows a narrow spectrum, with an intense origin transition followed by a three-member vibrational progression built on a 32 cm^{-1} mode. Vibronic bands of weaker intensity appear at 55 and 87 cm^{-1}.

The spectrum of the homochiral dimer consists of a series of weak bands starting at -73 cm^{-1} from the monomer origin and irregularly spaced, located on both sides of the monomer transition origin. The -73 cm^{-1} band is the most intense and can be taken as a transition origin. However, it is not possible to recognize the vibrational pattern of the bare molecules in that of the complex. Bands of lower intensity arise either from the activity of intermolecular modes, from the coexistence of different structures or from the existence of two electronic transitions because of the presence of two chromophores.

The shift of the electronic transition of the homochiral dimer is quite moderate for an aromatic dimer; they often show a red-shift of their electronic transition due to the increase of dispersion interaction upon electronic excitation.[58,60]

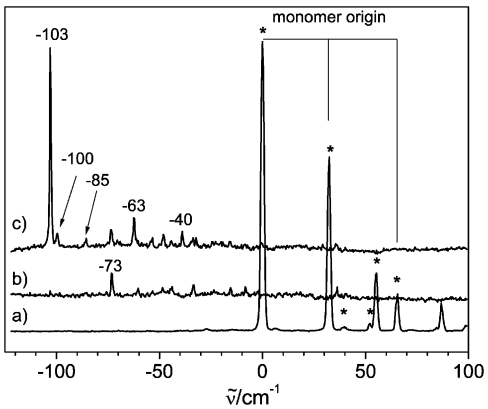

Fig. 3 S_0–S_1 spectrum recorded at the mass of (a) methyl mandelate (the bands marked with * are those probed in the IR/UV experiments), (b) methyl mandelate dimer (enantiopure sample), (c) methyl mandelate dimer (racemic mixture).

One can therefore suppose that the increase of dispersion in the excited state is partially counterbalanced by the decrease of electrostatic interactions.

When using a racemic mixture, the mass-resolved spectrum of the dimer shows an additional red-shifted and very intense band, about one order of magnitude stronger than the bands arising from the homochiral dimer. This difference in intensity tends to indicate an especially large stability of the heterochiral dimer in the pinhole nozzle expansion or a peculiar visibility due to high oscillator strength of the associated electronic transition.

The origin transition thus has two particularities when compared to what is observed in the homochiral dimer. First, it is more significantly red-shifted (-103 cm^{-1}) with respect to the transition origin. Such a red-shift is frequently observed in aromatic dimers like the anisole dimer.[61] It has been shown in purely dispersive systems that the red shift is more significant when the dimer has a stacked or parallel displaced geometry[62] than an extended geometry keeping the benzene rings far apart like in the benzonitrile dimer[63] or a T-shaped geometry.[64] In the dimer described here, hydrogen bonding can influence the shift of the electronic transition. The intense transition origin of the heterochiral dimer is followed by features of much weaker intensity, which again can be attributed to either the coexistence of several complexes or that of two electronic transitions. The second striking difference relative to the homochiral complex is the $\approx$10:1 ratio in the intensity of this band relative to the following ones, which contrasts with what has been observed for the FTIR spectrum, in which the intensity of the bands assigned to the homochiral dimer are of the same order as that assigned to the heterochiral dimer. We shall come back to this surprising difference later in the discussion.

3.2.3 Double resonance spectroscopy and comparison to FTIR spectroscopy. The IR-UV double resonance spectrum has been recorded setting the probe on different transitions of the methyl mandelate monomer (shown with * in Fig. 3). Whatever the transition probed, a single band appears at

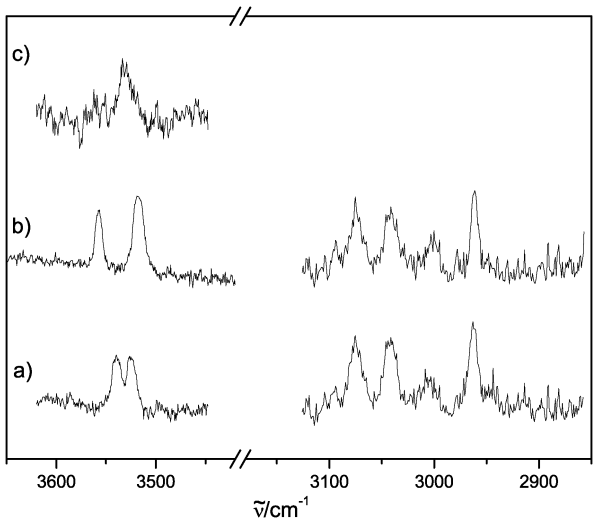

Fig. 4 Double resonance spectrum of the MM dimers with (a) probe at the homochiral dimer transition at -73 cm^{-1}, (b) probe at the heterochiral dimer transition at -103 cm^{-1}, (c) probe at the heterochiral dimer transition at -85.4 cm^{-1} (averaged on 4 scans).

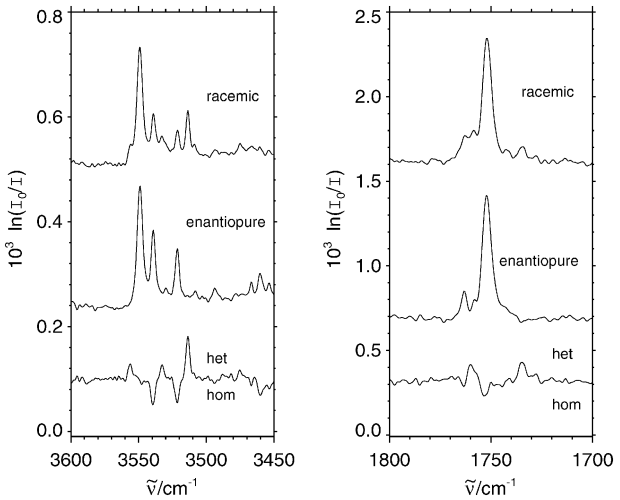

Fig. 5 Jet FTIR spectra of racemic and enantiopure samples of methyl mandelate and the difference of the two spectra in the O–H- and C=O-stretching regions.

3552 cm^{-1}, which clearly indicates the presence of a single monomer under the jet expansion conditions. To confirm this hypothesis, we also recorded the IR spectrum resorting to non-resonant ionisation detected IR spectroscopy,[65] with the UV probe set at -40 cm^{-1} from the monomer origin. Again, no other IR transition was detected.

The IR-UV spectrum of the homochiral dimer has been recorded by setting the probe on the band located at -73 cm^{-1} from the monomer origin (Fig. 4). Like the FTIR spectrum, this spectrum shows two bands of similar intensity, which are located at 3541 and 3522 cm^{-1} respectively (see Table 1).

The IR-UV spectrum of the heterochiral dimer has been recorded setting the probe on its absorption band at -103 cm^{-1}. Two narrow bands are observed, which consist of a blue- and a red-shifted peak with respect to the IR monomer origin. Their wavenumbers (3559 and 3518 cm^{-1}) are close to those observed in the FTIR spectrum (see Table 1). The spectra obtained by probing the bands located at -100 cm^{-1}, -63 cm^{-1}, -40 cm^{-1} are identical to that obtained when probing the band at -103 cm^{-1}. This shows that these bands belong to the same species as that responsible for the -103 cm^{-1} transition, or at least to a species with the same vibrational spectrum. In contrast, the spectrum obtained when the probe is set on the very weak heterochiral transition located at -85 cm^{-1} is completely different. Despite the signal to noise ratio being not as good as for the other bands, due to the low intensity of the probed band, a single band can be clearly distinguished at 3532 cm^{-1}. This band is also observed in the FTIR spectrum. However, it is far from being the dominant species in the S_0–S_1 spectrum, while its intensity is comparable with the other bands in the FTIR spectrum. Part of this may be attributed to the FTIR subtraction scheme as the band is close to the homochiral dimer band and is the weakest band in the racemic FTIR spectrum (top trace of Fig. 2), but experimental artifacts are not large enough to explain this difference. The resulting peak wavenumbers are summarized in Table 1. Wavenumber discrepancies between FTIR and IR/UV bands are typically within 4 cm^{-1} and mostly reflect the $\approx$2 cm^{-1} bandwidth of the IR OPO used in the experiment.

An advantage of the FTIR technique is that one can easily move to another spectral range to correlate the chirality recognition phenomena probed by different functional groups. This is shown in Fig. 5 for the C=O stretching region. The clustering effects are much weaker, because the monomer dominance in the expansion is not masked by an IR intensity enhancement due to hydrogen bonds. Nevertheless, one can see at least two heterochiral and one or two homochiral contributions close to the monomer band. Their positions are listed in Table 1. Due to the much weaker intensity dependence of the C=O stretching modes on hydrogen bonds, the spectra underscore that similar quantities of homo- and heterochiral clusters are formed in the racemic slit jet expansion.

In the C–H stretching range (see Fig. 2 and Table S1 in the supplementary information†), no significant FTIR differences between enantiopure and racemic expansions can be found. This does not rule out conformation and chirality recognition effects involving C–H bonds,[19] because the cluster concentration in the expansion is low and the C–H stretching range does not profit as much from signal enhancement through hydrogen bonding as the O–H stretching range. Fig. 4 provides dimer-specific spectra, a substantial advantage of the IR/UV double resonance technique. They show the absence of significant differences between homo- and heterochiral dimers in the C–H stretching range. The corresponding monomer-specific spectra are shown in Fig. S1 (supplementary information). They confirm that relative IR intensities are reproduced reasonably well by the IR/UV technique within a given spectral range. Differences in the fingerprint region (see Fig. S1) are also small and somewhat difficult to detect due to the weakness of the IR transitions.

3.3 Quantum chemical calculations

The systems studied here involve aromatic species, which are highly polarisable. Dispersion is expected to play an important role in the structure and the binding energy of the complexes. We shall therefore limit ourselves here to the results obtained with methods which take dispersion into account. We describe the calculations obtained with correlated methods like MP2/6-31G** or MP2/6-31+G*, as well as those obtained at the RI-B97-D/def2-TZVP level. The results obtained at the B3LYP level are given in the supplementary information† to exemplify the failure of this method to predict the energetically favorable dimer structures (see Table S3 and Fig. S4, S5 in the supplementary information), whereas the monomer description (Table S2, supplementary information) is satisfactory.

3.3.1 Monomers. The methyl mandelate monomer has recently been studied at the B3LYP/6-31G** and MP2/6-31G** level[24] and we only add here some results at other levels of approximation which are applied to dimers in the present work. The $\approx$9 kJ mol^{-1} energy difference between the global minimum structure (SsC, O–H in Syn conformation bonded to the O=C group) and the locally stable structure (GskC, O–H in Gauche conformation bonded to the O–CH_3 group) is similar at MP2 and B3LYP levels (see Fig. 6, Table S2 in the supplementary information† and ref. 24). It is sufficiently large for a dominance of the SsC structure in supersonic jet and matrix isolation spectra, and already at room temperature.

In Fig. 7, the harmonically predicted spectra of the two conformations are compared to the experimental matrix isolation spectrum, which offers a wider frequency coverage and better signal to noise ratio than the jet spectra. The agreement with the SsC prediction is better and like in the UV spectra there is no evidence for a significant contribution from the less stable isomer. We note, however, that such higher-lying isomers have been tentatively postulated in matrix isolation studies of methyl lactate.[26]

The SsC global minimum structure has an intramolecular H···O hydrogen bond distance of 205.5 pm, 1% shorter than in methyl lactate (B3LYP/6-31+G*). The main difference between the two systems is that the isomerization barrier

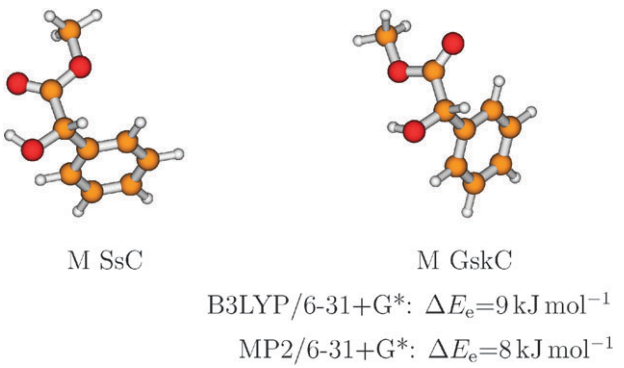

Fig. 6 Calculated methyl mandelate monomer (M) conformations SsC and GskC at the MP2/6-31+G* level together with electronic energy differences. SsC involves an internal hydrogen bond to the carbonyl group and is significantly more stable.

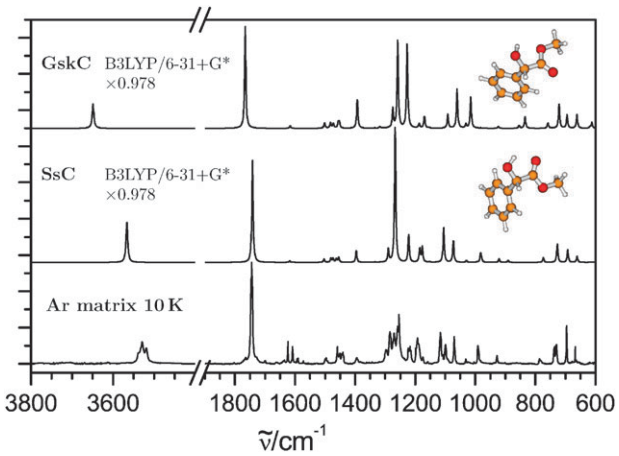

Fig. 7 Experimental FTIR spectrum of methyl mandelate in an argon matrix (10 K) and B3LYP/6-31+G* calculated spectra of the SsC and GskC monomers. The calculated spectra were simulated using Lorentzian functions with a half-bandwidth of 5 cm^{-1}. Wavenumbers are scaled by 0.978, a compromise for the gas phase OH and C=O bands, which also explains why the matrix OH band is red-shifted.

between the SsC and GskC conformers is higher in methyl mandelate than in methyl lactate (19 kJ mol^{-1} *vs.* 16 kJ mol^{-1}, B3LYP/6-31+G*). The difference between the potential energy surfaces of the two molecules is further analyzed in the supplementary information (see Fig. S2 and S3 in the supplementary information†).

The harmonic wavenumber prediction for the SsC monomer conformation depends on the employed methods, because of anharmonicity and sensitivity of hydrogen bond description to the basis set. It is smaller when calculated at the MP2 or B3LYP level using the 6-31+G* basis set with diffuse functions (3645 and 3647 cm^{-1}, respectively; Table S2 in the supplementary information†) than when using the 6-31G** basis set (3783 and 3699 cm^{-1};[24]). The difference to the experimental value of 3549 cm^{-1} is largely due to anharmonicity.[66] Inadequate description of the hydrogen bond can also play a role. The GskG monomer OH stretch is predicted 70–80 cm^{-1} higher in wavenumber, in agreement with the circumstantial evidence from the matrix isolation spectra. For the C=O stretching fundamental, where the anharmonicity constant is much smaller and can be estimated from overtone observations[22] around 10 cm^{-1}, the harmonic MP2 and B3LYP predictions are much closer to the experimental harmonic estimate of $\approx$1770 cm^{-1} than the B97-D prediction of 1724 cm^{-1}. This is a typical deficiency of semi-local (non-hybrid) density functionals which is of course not remedied by the empirical dispersion term. Again, the predicted position of the GskC isomer C=O stretch is in agreement with the circumstantial evidence from the matrix isolation spectrum.

3.3.2 Dimers. Dimer calculations are substantially more challenging than monomer calculations in the case of methyl mandelate. Adding to the more or less steep increase of computational cost with system size, conventional density functional and also MP2 calculations are known to be quite inadequate for the description of π–π interactions. While hybrid functionals like B3LYP do not capture this interaction

at all,[67,68] the MP2 level overestimates them.[69–71] At the computational levels employed here, the benzene dimer has an electronic binding energy between 2 kJ mol^{-1} (B3LYP/6-31+G*) and 25 kJ mol^{-1} (MP2/6-31+G*), whereas high level estimates based on CCSD(TQ) extrapolations[18] lead to 11.4 kJ mol^{-1} (10.3 kJ mol^{-1} including estimated zero point energy weakening effects). The B97-D/def2-TZVP result for D_e is 12.1 kJ mol^{-1}. The experimental value of the dissociation energy is discussed in ref. 72 and ranges between 6 and 12 kJ mol^{-1}.[73,74] For the quantum chemical calculations of the MM dimers reported here, only the most stable SsC monomer with an internal OH···O=C hydrogen bond was considered because it dominates in our experimental conditions.

3.3.3 Structure and energetics. A systematic screening of possible structures as outlined in section 2.7 at MP2/6-31G** level was carried out (see Table 2). If one considers a limit for hydrogen bonding of about 2.2 Å, it is relatively easy to classify these structures according to their hydrogen bond topology, into four classes. The 8-ring structures sacrifice their intramolecular hydrogen bonds in favor of intermolecular ones. The 5-ring structures do the same but keep one relatively short intramolecular contact. The 4-ring structures conserve one weak intramolecular hydrogen bond and form one intermolecular bond. Dispersion-bound 44-ring structures keep both of their intramolecular hydrogen bonds. The intra- and intermolecular hydrogen bond distances at different levels of theory are listed in Table S4 in the supplementary information.†

3.3.4 Double hydrogen-bonded structures. We shall first discuss the 8-ring and 5-ring structures, which both involve two intermolecular hydrogen bonds. These dimer structures resemble those postulated for methyl lactate.[11,75] We encode the relative monomer configuration and the hydrogen bonded ring size in these dimers by Hom/Het and 8/5, thus labelling the structures Hom8, Hom5, Het8 and Het5. The 8-ring structure is analogous to the most stable methyl lactate dimer and forms a ring of 8 heavy atoms with two isolated OH···O=C hydrogen bonds (8-dimer).[11,75] Variants of this structure, with different symmetry groups, are found for the homochiral as well as the heterochiral complex. Some have no symmetry (see Hom8a in Fig. 8), but homoconfigurational pairing is compatible with C_2 symmetry and is indeed found for two Hom8 structures, namely Hom8b and Hom8c, which differ in the twist or axial chirality of the flexible 8-ring (see Fig. S4 in the supplementary information†). This ring flexibility leads to almost perpendicular arrangements of the two hydrogen bonds, which may be classified similar to substituted allenes. According to the IUPAC rules for axial chirality Hom8c can be denoted with the chirality descriptor R_a and structure Hom8b with the chirality descriptor S_a. Hom8b lends itself well to π–π interactions and is the most stable structure, keeping the C_2 symmetry constraint (see Table 2). Dispersion plays an important role in binding this structure, which explains that B3LYP reproduces neither its outstanding binding energy nor the phenyl–phenyl distance (see Table S3 and S4 in the supplementary information). In contrast to this, the Hom8c structure does not profit from dispersion interactions, because the distance between the phenyl rings is larger than in Hom8b (see Table S4 in the supplementary information). The Hom8a and Hom8b dimers only differ in the orientation of the phenyl rings. In the Hom8a dimer the phenyl ring arrangement is T-shaped, thus breaking the C_2 symmetry. Both homochiral 8-ring structures have similar binding energy; such that it is only possible to differentiate between them based on spectroscopic data (see below).

C_i symmetry is compatible with a heteroconfigurational pairing and is indeed found for the Het8a structure (Fig. 8). It should be noted that the homochiral 8-ring structures are systematically more stable than the heterochiral 8-ring dimers, by at least ≈5 kJ mol^{-1}. One reason for this is that two homoconfigurational monomers can bring together the two phenyl rings without sacrificing the two intermolecular hydrogen bonds in a Hom8 structure, whereas two mirror-image monomers cannot, thus leading to a less stable Het8a structure. The heterochiral Het8b structure without inversion symmetry allows for interactions between the phenyl ring and the ester group but is also not competitive.

The 5-ring structures found here are also reminiscent of what has been postulated for the methyl lactate dimer. They consist of a ring of 5 heavy atoms where the O–H group of one molecule is inserted into the intramolecular hydrogen bond of the other molecule, thus forming cooperative OH···OH···O=C hydrogen bonds (5-dimer).[11] The 5-ring structures do not have point group symmetry elements. The Hom5 structures can be of similar stability as the Hom8 dimers (Table 2). They profit less from dispersion. The case of the heterochiral dimer is slightly different. Among the heterochiral dimer structures, Het5 allows for a close contact of the phenyl groups, which favors dispersion and makes it

Table 2 Most stable homo- and heterochiral dimers at MP2/6-31G** level with electronic dissociation energies D_e in kJ mol^{-1} including 50% counterpoise correction (CPC) and dissociation energies without CPC correction, obtained by a systematic search as described in section 2.7. Also given are MP2/6-31+G* and B97-D/def2-TZVP dimer dissociation energies for some of the most stable structures with different topology. The structures are sorted by hydrogen bond topology and the largest binding energies for homo- and heterochiral dimers are highlighted in bold face

	MP2/6-31G**		MP2/6-31+G*	B97-D/def2-TZVP
	D_e + 50%CPC	D_e	D_e	D_e
Hom8a	41.4	**61.9**	**77.1**	**44.9**
Hom8b	41.0	58.5	72.2	44.8
Hom8c	37.8	57.5	59.9	39.4
Hom8d	41.4	61.5	—	—
Hom4	39.6	55.9	72.0	41.4
Hom4b	33.1	49.3	—	—
Hom44a	34.1	54.6	68.4	42.5
Hom44b	35.0	50.3	—	41.7
Hom5a	**41.6**	60.1	—	40.4
Hom5b	33.7	48.5	55.8	37.7
Het8a	34.0	50.8	59.7	40.6
Het8b	35.8	53.3	59.8	37.7
Het4	**45.9**	**67.5**	**79.6**	**50.7**
Het4b	35.5	48.0	—	—
Het44a	34.0	52.5	67.1	43.4
Het44b	36.3	54.6	74.4	41.3
Het5	39.1	57.5	69.6	43.2

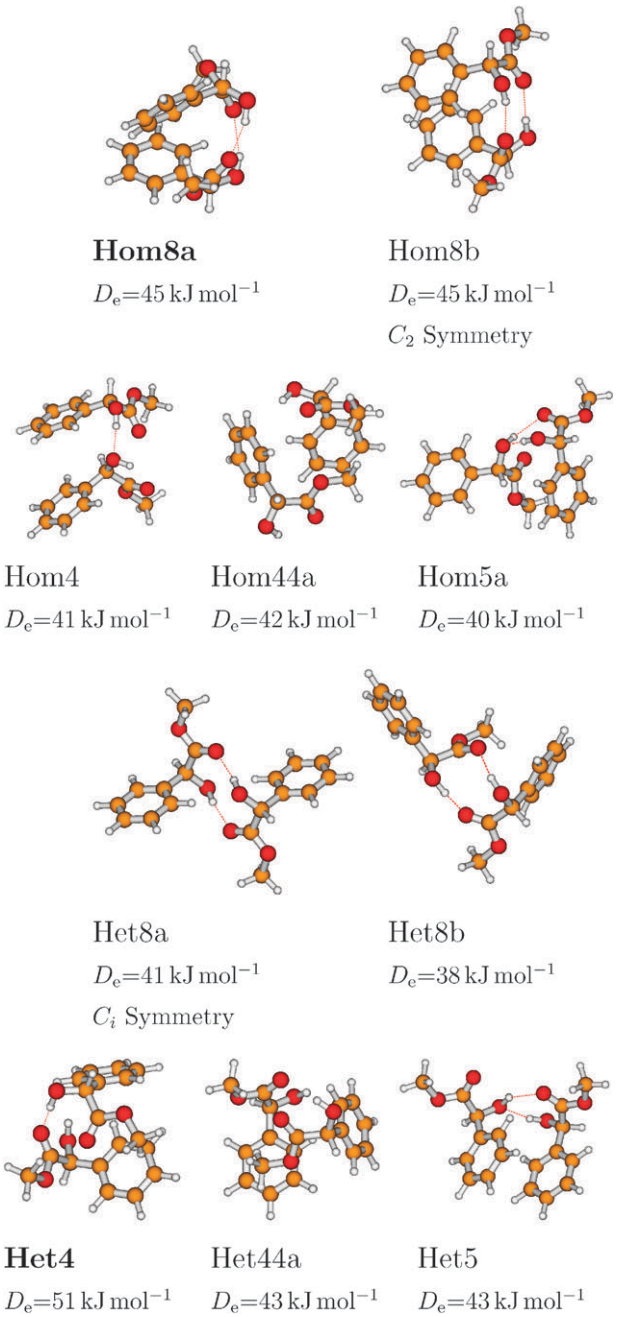

Fig. 8 Structures of the calculated homo- and heterochiral dimers with different topology optimized at the B97-D/def2-TZVP level. Bold face indicates the tentative assignment to the experimental spectra.

more stable than Het8a. Based on doubly hydrogen bonded structures alone, one would thus expect Hom8a and Het5 to dominate the expansion—two different hydrogen bond connectivities which both optimize π–π interactions.

3.3.5 Single hydrogen-bonded and purely dispersion-driven structures. In contrast with what was observed for the methyl lactate dimer, the influence of phenyl–phenyl interactions allows new aggregation topologies to energetically compete with the 5-ring and 8-ring structures. In what we call 4-ring dimers, only one classical OH···O hydrogen bond is formed between the two monomer units. The second monomer unit retains its intramolecular hydrogen bond, which involves 4 heavy atoms (OCCO) instead of closing an intermolecular hydrogen-bonded ring. The resulting Het4 dimer is indeed the most stable heterochiral dimer structure and even the most stable of all calculated dimer structures at MP2 level. This is confirmed at DFT-D level (Table 2). The two phenyl rings arrange themselves in a T-shaped structure, similar to the one in the benzene dimer. The Het4 dimer is stabilized by ≈10 kJ mol^{-1} relative to the second more stable heterochiral dimer (MP2/6-31G** and MP2/6-31+G*). In contrast, Hom4 is not the most stable homochiral dimer.

There is an even more drastic possibility: in what we call 44-ring dimers, neither of the monomers opens its intramolecular (4-ring) hydrogen bond and there is thus no classical hydrogen bond between the two monomers. This topology is largely driven by dispersion interactions. Such structures are not at all competitive at B3LYP level (see Table S3 in the supplementary information†) but become competitive or even superior to classical hydrogen bond structures in MP2 calculations (see Table 2). Het44 structures, for which we present one example in Fig. 8, are more stable than Het8 but do not reach the stability of the Het4 structure.

It can be concluded that a particular heterochiral dimer structure, namely Het4, clearly predominates energetically. The large degree of chirality discrimination due to the phenyl interactions is evident from the fact that Hom4 is not among the four most stable homochiral dimers. One reason for that peculiar stability of Het4 is the optimal combination between the formation of a single intermolecular hydrogen bond and optimization of dispersion. The trade-off is to break one hydrogen bond, to bring the two phenyl rings together, and to exploit the dangling hydrogen bond valences for secondary interactions. This is what the compact Het4 structure achieves.

3.3.6 Influence of the basis set. The most stable dimers have been in part re-optimized and in part found independently at the MP2/6-31+G* level to estimate the influence of the basis set on the structure and energetics of the complexes and the completeness of the conformational search. All the binding energies are shifted up. The peculiar stability of Het4 is maintained with a similar difference in binding energy (≈10 kJ mol^{-1}) relative to the second most stable heterochiral dimer whereas the difference between homochiral and heterochiral interaction energies tends to decrease somewhat. As both basis sets must ultimately be considered inadequate for quantitative MP2 binding energies, we refrain from an extended discussion. A future estimate of the MP2 basis set limit for this interesting model system is strongly encouraged.

3.3.7 Frequency calculations. Harmonic frequency calculations at the canonical MP2 level are prohibitively expensive. This calls for a dispersion-augmented DFT method such as B97-D/def2-TZVP.[54] The method has proven to yield results of almost CCSD(T) quality in numerous studies of non-covalent interactions including conformation problems of various type (for selected references see ref. 76–79). Some vibrational spectra have recently been successfully studied in ref. 80. The structures described above have been re-optimized at this level. Visually, they are not easily distinguishable from

Table 3 DFT-D dimer dissociation energies (D_0) with zero point energy correction and calculated harmonic OH and CO stretching wavenumbers ω/cm^{-1} (band strengths I/(km mol^{-1})) for the OH and C=O stretching vibrations

B97-D/ def2-TZVP	D_0 kJ mol^{-1}	ω(OH) cm^{-1}	I km mol^{-1}	ω(CO) cm^{-1}	I km mol^{-1}
M SsC	—	3637	67	1724	211
D Hom8a	**36.8**	3623	184	1727	307
		3601	206	1732	152
D Hom8b	36.7	3585	562	1723	78
		3581	7	1722	442
D Hom8c	32.8	3566	1004	1718	492
		3548	40	1711	91
D Hom4	34.2	3588	98	1737	254
		3428	581	1726	182
D Hom44a	36.6	3644	122	1735	215
		3628	59	1721	158
D Hom44b	36.5	3640	77	1722	281
		3615	70	1721	136
D Hom5a	33.6	3545	335	1740	142
		3427	495	1731	247
D Hom5b	30.5	3544	468	1742	169
		3465	339	1714	300
D Het8a	33.8	3517	1029	1720	694
		3500	0	1714	0
D Het8b	23.0	3586	522	1721	457
		3472	486	1710	168
D Het4	**41.5**	3658	122	1740	209
		3564	235	1715	282
D Het44a	37.2	3658	141	1738	211
		3614	65	1720	175
D Het44b	36.7	3626	83	1725	254
		3601	81	1718	157
D Het5	34.6	3559	375	1744	163
		3486	337	1719	253

the corresponding MP2/6-31+G* structures despite significantly different binding energies (see Fig. 8, Table 2). Small differences occur in the hydrogen bond distances, which tend to be slightly longer at the B97-D/def2-TZVP level (see Table S4 in the supplementary information†). The energetic and spectral predictions at DFT-D level are summarized in Table 3.

The good correlation between DFT-D and MP2 dimer energetics (Table 2) is underscored by Fig. S5 in the supplementary information†, in which the electronic dissociation energies of the B97-D dimers are plotted against the corresponding MP2 energies. We should note however that MP2 and DFT-D differ in the relative importance of 5-ring and 44-ring structures but agree in the 4-/8-ring switchover between homochiral and heterochiral dimers (Table 4).

The spectral predictions for the most stable topologies are compared to the experiment in Fig. 9 and 10. This comparison deserves several comments. First, depending on their symmetry, the spectrum of the calculated complexes shows a single IR-active band or two distinct bands. In the Hom8a dimer the phenyl ring arrangement is T-shaped, thus breaking the C_2 symmetry. This results in two intense bands in the OH stretching region, whereas only one intense band is predicted for the symmetric Hom8b dimer. Both structures have similar binding energy, such that it is only possible to differentiate between them based on spectroscopic data. One should also note that 44-ring structures suffer from a 3–7 times poorer O–H visibility than 8-ring and 5-ring structures, because the intramolecular hydrogen bond is strained and shows a weaker dipole moment derivative enhancement than the intermolecular ones. This is much less the case in the C=O stretching region such that these associated structures are more likely to be detected in that range. Keeping this in mind, we can compare the calculated and experimental IR spectra.

We shall first discuss the case of the homochiral complex. As mentioned above, there are several structures of similar binding energy, which can be discriminated only on the basis of spectroscopic data. The B97-D/def2-TZVP OH stretching

Table 4 Qualitative sequence of the most stable structures (dissociation energy without zero point energy correction (D_e)) for a given hydrogen bond topology at different levels of approximation. B3LYP shows no sensitivity to chirality, MP2 reverts the heterochiral 8-/4-ring preference and DFT-D in addition tends to favor 44-ring structures over 5-ring structures. For the absolute B3LYP dissociation energy values see Table S3 in the supplementary information

	Hom	Het
B3LYP	8 > 5 ≈ 4 > 44	8 > 5 > 4 > 44
MP2	8 > 5 ≈ 4 > 44	4 > 5 ≈ 44 > 8
DFT-D	8 > 44 > 4 > 5	4 > 5 ≈ 44 > 8

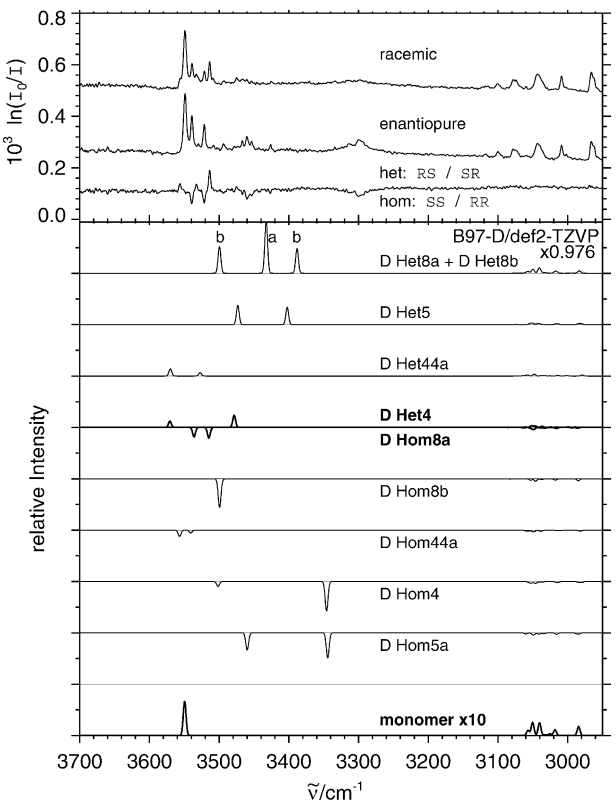

Fig. 9 Upper part: Popcorn-jet spectra of the racemate (T_{sample} = 363–373 K, 2000 co-added spectra) and the *S* enantiomer (T_{sample} = 363–373 K, 1800 co-added spectra) of methyl mandelate in the OH stretching region and the difference of the two spectra with the bands of the heterochiral (het) clusters pointing upwards and the bands of the homochiral (hom) clusters pointing downwards. Lower part: Simulated spectra for the monomer, the homochiral dimers (inverted for a better comparison to the experimental difference spectrum) and the heterochiral dimers from the calculated wavenumbers at DFT-D (B97-D/def2-TZVP) level, scaled by 0.976, including also the C–H region which is weaker and more sensitive to details of the intramolecular dynamics than to intermolecular recognition.

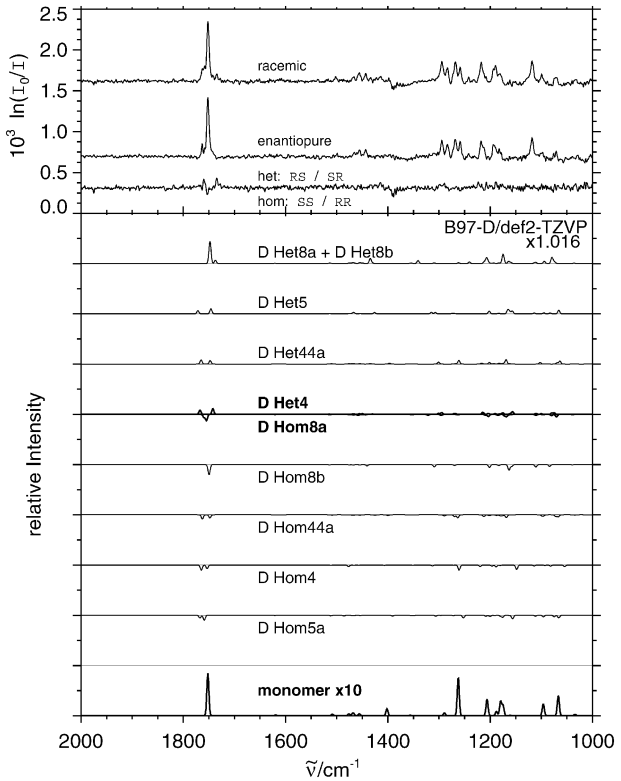

Fig. 10 Upper part: Popcorn-jet spectra of the racemate (T_{sample} = 363–373 K, 700 co-added spectra) and the *S* enantiomer (T_{sample} = 363–373 K, 1000 co-added spectra) of methyl mandelate in the carbonyl stretching region and the difference of the two spectra with the bands of the heterochiral clusters pointing upwards and the bands of the homochiral clusters pointing downwards. Lower part: Simulated spectra of the carbonyl stretching vibration for the monomer, the homochiral dimers (inverted for a better comparison to the experimental difference spectrum) and the heterochiral dimers from the calculated wavenumbers at B97-D/def2-TZVP level, scaled by 1.016, including also the fingerprint region which is weaker and more sensitive to details of the intramolecular dynamics than to intermolecular recognition.

red-shift predictions for the 5-ring structures are by far too large, thus confirming that these structures cannot be at the origin of the experimentally observed dimer features. This remains valid if one takes into account that pure density functionals tend to overestimate such shifts even more than hybrid functionals.[81] The red shift of the hydrogen-bonded OH of methanol dimer relative to the monomer may serve as a pronounced example. Experimentally, it is 111 cm^{-1},[66] whereas it is predicted to be 191 cm^{-1} at the B97-D/def2-TZVP level. B3LYP and MP2 calculations only overestimate the dimer shift by 30–50%. For the cooperative methanol trimer, these methods predict shifts within 15% of the experimental value,[66] whereas the B97-D/def2-TZVP shift is still overestimated by about 40%. Furthermore, the spectrum of the homochiral dimer shows a doublet and cannot be interpreted in terms of the Hom8b structure. The best agreement between experiment and theory is found for the most stable homochiral dimer Hom8a. We therefore assign the doublet observed in the FTIR spectrum of the homochiral dimer to Hom8a.

The case of the heterochiral complex is more straightforward as the Het4 structure dominates energetically and its spectrum reproduces well two out of the three bands observed in the spectrum of the heterochiral dimer. It should be noted that none of the 5-ring or 8-ring dimers shows a blue-shift of one of its OH stretching frequencies, in contrast with most of the 4-ring or 44 dimers. This reinforces our assignment. However, a third band of the heterochiral complex spectrum remains unassigned. At this stage, it may be interesting to compare the results obtained by different methods, direct absorption or IR-UV double resonance spectroscopy. The conformer-specific IR-UV double resonance experiments show that the band observed at 3532 cm^{-1} is broader than the bands observed in the other spectra and could correspond to a congested doublet. The additional band for the heterochiral clusters may thus arise from a heterochiral 44-ring structure. Without connecting hydrogen bonds, it profits from a reduced zero point energy destabilization and it may form from stable monomers without significant activation barrier. However, this assignment must be considered more tentative than the others.

The Hom8a/Het4 assignment is fully confirmed in the difference spectrum of the C=O stretching mode (Fig. 10). Although weak due to the missing hydrogen bond enhancement, the heterochiral part rules out an 8-ring assignment, whereas the homochiral part rules out a Hom4 assignment. Specifically, the blue-shifted heterochiral band at 1760 cm^{-1} must be due to the non-hydrogen-bonded C=O group, which emerges from the optimization of dispersion interactions. The band at 1763 cm^{-1} is somewhat more prominent in the enantiopure expansion and likely due to larger OH-connected ring cluster contributions, as in the case of methyl lactate.[11] All together, and neglecting these minor contributions from larger clusters, the simulations are consistent with $\approx$80% monomer and $\approx$20% dimer in the FTIR-probed region.

At this stage, it is rewarding to come back to the UV spectra and to compare the information gained from the FTIR spectrum and the results obtained by double resonance spectroscopy. They show two major differences. The first one is the prominence of the heterochiral band assigned to Het4 in the S_0–S_1 spectrum, which is more intense by one order of magnitude than all the other bands. In contrast, Het4 appears with similar intensity as the other complexes in the FTIR spectrum. The second important difference is that the heterochiral complex responsible for the band at 3532 cm^{-1} in the IR is clearly distinguishable in the FTIR absorption spectrum but is hardly seen in the S_0–S_1 spectrum at -85 cm^{-1} from the monomer origin.

One should not dismiss first that the ionization detected UV spectra of MM dimers may have some intensity effects (strong -103 cm^{-1} band, weak -85 cm^{-1} band, or strong heterochiral transition origin, weak homochiral one) which do not only reflect population differences. Indeed, variations in the UV oscillator strengths or Franck–Condon factors and radiationless processes may influence the relative intensity of the bands. The oscillator strength of the electronic transitions is not expected to vary a lot upon dimerization, as long as the electronic transition is localised. If the transition is delocalised, different coupling schemes between the two electronic

transition moments of the two sub-units may increase the oscillator strength by a factor of up to two in the heterochiral complex relative to the homochiral complex. The difference in geometry between the homochiral complex and the heterochiral adduct could explain different coupling schemes. Similarly, the larger red-shift of the electronic transition of the heterochiral complex must be related to a weaker contribution of the electrostatic forces which often decrease in the electronic excited state when the chromophore is a benzyl-alcohol derivative.[82,83]

However, such arguments are not sufficient to explain the ≈10:1 intensity ratio between the transition origins of the heterochiral and homochiral complexes, and between the −103 and −85 cm^{-1} bands. The very high intensity of the heterochiral contribution to the S_0–S_1 spectrum may thus reflect an outstanding stability of Het4 although it is surprising that it does not show up in the FTIR spectra to such an extent. On the contrary, the same quantity of heterochiral and homochiral dimers seems to be formed in the slit jet, as reflected by the statistical dimer intensity drop by a factor of two when switching from enantiopure to racemic expansions. This is in line with expectations for irreversible dimerization processes, *i.e.* sticking coefficients close to one or at least similar to each other. Due to the much weaker intensity dependence of the C=O stretching modes on hydrogen bonds, this spectral region can be used to underline that similar quantities of homo- and heterochiral clusters are formed in the racemic slit jet expansion.

The observed difference between the double-resonance and FTIR spectra could be linked to the fact that different cooling conditions in the pinhole nozzle and in the slit jet may favor different complexes. Comparison between the aperture size and backing pressures in the two experiments show that the slit jet corresponds to warmer conditions. Moreover, the FTIR spectrum is recorded much closer to the nozzle (about 2–10 mm) than the double resonance spectrum (150 mm). Warmer conditions in the slit jet would allow a less stable heterochiral isomer to be observed.

The much smaller intensity of the complex responsible for the band at 3532 cm^{-1} in the IR and −85 cm^{-1} in the UV spectrum could be explained by fast non radiative processes. On the other hand, this complex might involve a particularly strong hydrogen bond, which endows it with a particularly high visibility in the FTIR spectrum, because IR band strengths are sensitive to hydrogen bonding. However, this should also enhance the IR/UV action spectrum and would be expected to lead to a stronger IR red-shift. Moreover, Fig. 9 shows that the dimers we observed belong to the least visible ones in terms of their OH stretching intensity. This underlines the competition which hydrogen bonding experiences from the aromatic interaction, because strong hydrogen bonds typically lead to substantial OH stretching enhancement.

Although the details of the dimer assignments may still change with higher level quantum-chemical treatments, it is clear that methyl mandelate dimers exhibit strong chirality discrimination effects. Inclusion of dispersion opens the way for a plausible interpretation of the MM dimer IR spectrum in terms of the most stable structures, consistent with thermodynamically controlled cluster reorganization. Depending on the relative chirality of the two monomer units, radically different hydrogen bond topologies are formed. While homoconfigured monomers form double hydrogen bonds, heteroconfigured units only form one, and even perhaps no classical intermolecular hydrogen bond at all in some minor fraction. The driving force for this difference is an optimization of the contact between the two phenyl rings. Such a contact is more compatible with hydrogen bonding in the homochiral case. Chirality recognition driven by optimization of dispersion is made possible in this particular system by the fact that intermolecular and intramolecular hydrogen bonds are of similar energy. The gain in energy when opening an intramolecular hydrogen bond to form an intermolecular bond is not decisive. It may be energetically rewarding to optimize London dispersion instead.

An alternative view on MM dimerization regards it as dispersion driven combination of substituted benzenes.[84] If the stereochemistry and cooling process allow for it, the substitutents rearrange to form one or two intermolecular hydrogen bonds at the price of intramolecular variants. The UV and IR spectra catch the spectroscopic signature of this secondary process.

3.4 Larger clusters and bulk solids

In the jet-FTIR spectra, absorptions from larger clusters are observed to lower wavenumber. By comparison with the methyl lactate case,[11] these clusters can be tentatively assigned as trimers (T) and cyclic tetramers and larger clusters (C). Fig. 11 shows a comparison of methyl mandelate and methyl lactate jet-FTIR spectra. The MM monomer is further red-shifted, in line with the somewhat stronger hydrogen bond. The dimer bands are more complex and more red-shifted in methyl lactate than in methyl mandelate. This complexity is most likely due to coupling of the OH stretching modes with twisting motions of the 8-ring or to the co-existence of different isomers, but it remains to be analyzed quantitatively. The phenyl ring interactions presumably quench these twisting modes. The reduced dimer red-shift may also be traced back to the phenyl group interactions, which compete with optimum hydrogen bond arrangements. In view of these differences for monomers and dimers, the similarity between enantiopure methyl mandelate and methyl lactate for larger clusters is striking. Both compounds exhibit a relatively strong absorption near 3460 cm^{-1} (T), which was attributed to a cyclic trimer with OH···OH bonds in the case of methyl lactate.[11] The same assignment is likely for methyl mandelate. One reason why the MM band is broader could be a Fermi resonance with the C=O stretching overtone state, which is predicted to be very close in energy (see section 3.1). In the region of 3300 cm^{-1}, enantiopure methyl lactate shows a broad doublet band, which is attributed to cyclic tetramers and possibly also larger clusters with the same OH···OH hydrogen bond pattern (C). The same is most likely the case for methyl mandelate, which exhibits a single broad band near 3300 cm^{-1}.

A remarkable difference between methyl lactate and methyl mandelate may be noted in the racemic case. Racemic methyl lactate expansions show a sharp tetramer band (Q) in between

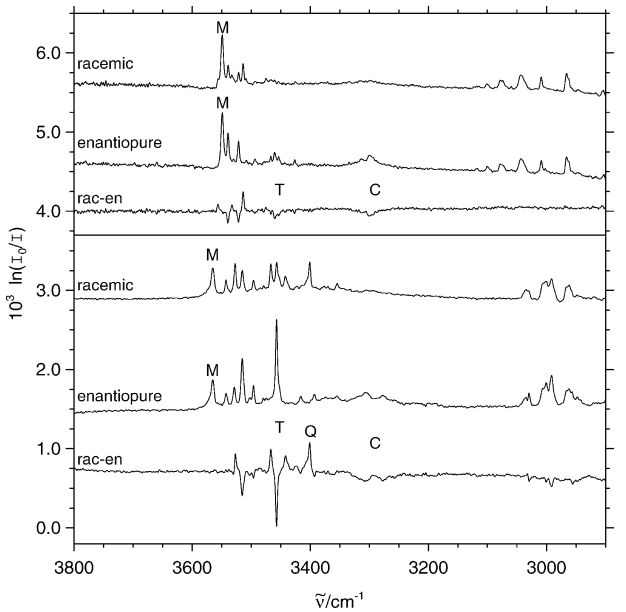

Fig. 11 Popcorn-jet FTIR spectra of racemic and enantiopure MM together with their difference (top traces, multiplied by 3) compared to ragout-jet FTIR spectra of MLac[11] (bottom traces). Monomer (M), trimer (T) and tetramer/oligomer (Q, C) absorptions are marked, whereas unlabelled regions correspond to dimers.

the T and C bands. This band has been attributed to a cyclic *RSRS*-tetramer with alternating chirality and a unique OH···O=C hydrogen bond pattern.[10] This structure was furthermore shown to be very sensitive to chirality mismatches in the cyclic arrangement. Such a spectral feature is completely absent in the racemic methyl mandelate spectrum (top trace in Fig. 11). A straightforward explanation is that the OH···O=C-connected tetramer is not energetically competitive for MM, either because the phenyl groups make it sterically unfavorable or else because they offer attractive secondary interactions in OH···OH-connected tetramers. The latter explanation appears more likely, because the steric hindrance of the phenyl group in the Q structure is not critical. The stronger clustering propensity of the enantiopure expansion may point in the same direction. In the cyclic clusters, all phenyl groups are then on the same side and can interact most intensely. However, systematic quantum chemical studies will be needed to elucidate these observations. Already without structural rationalization, the observations confirm the singularity of the lactate case in terms of chirality recognition.[1]

Finally, the spectral evolution towards the bulk phases of MM shall be investigated. In Fig. 12 a comparison of methyl mandelate in different states of aggregation is shown. Only for the jet expansion and for the crystalline solid did the enantiopurity have an effect on the spectra. As the matrix and glassy state spectra look similar for the racemate and the enantiopure sample, only the enantiopure sample is presented. The annealed Ar matrix spectrum shows the strongest OH stretching red shifts. Although the band is much broader, it corresponds in position to the C band of mandelate tetramers in the jet and is most likely dominated by extended chains of cooperative hydrogen bonds between the α-OH groups. The glassy spectrum has a much reduced red-shift, although it was recorded at a lower temperature. This must be attributed to a significant fraction of monomer-(and possibly dimer-)like OH···O=C hydrogen bonds, as these are expected when the molecules are quenched on the cold substrate without being able to rearrange. The dispersion interactions contribute to the metastability of this randomly packed ensemble of molecules. Upon warming the glassy state, the molecules can rearrange and alcoholic hydrogen bonds can start to form. Therefore, the OH stretching band is further red-shifted despite the temperature increase. After re-cooling its red-shift comes close to that of the annealed matrix spectrum and the band narrows. The room temperature crystalline state also shows a narrow band because of the increased order, but the band center is further blue-shifted due to the increased thermal weakening of the hydrogen bonds. The crystalline spectrum agrees well with the one reported earlier.[23] However, in that work, no investigation of enantiopurity effects was carried out.

In Fig. 13, we compare ATR spectra of enantiopure and racemic crystalline methyl mandelate in selected regions, where significant spectral differences are observed. Most of the bands of the enantiopure sample are systematically blue-shifted relative to those of the racemic compound. The band near 780 cm^{-1} represents an exception, being slightly red-shifted in the enantiopure compound. Based on quantum-chemical monomer and dimer calculations, this band may be assigned to a complex backbone vibration, which is coupled to out-of-plane C–H vibrations of the aromatic ring. The latter exhibit their main band near 740 cm^{-1}, which is substantially more structured in the crystals of the racemic mixture. This points at a different phenyl group arrangement and possibly also a differently sized unit cell. Such a difference in the crystal packing is confirmed by systematic spectral shoulders on the

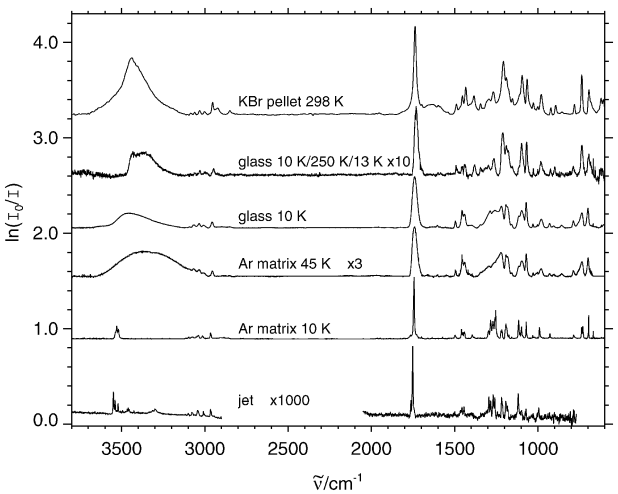

Fig. 12 FTIR spectra of enantiopure methyl mandelate in different aggregation states (from bottom to top): jet spectrum (×1000), matrix spectrum after deposition (10 K), matrix spectrum after annealing (45 K, ×3), glassy state spectrum as deposited (10 K), glassy state spectrum after annealing (to 250 K) at 13 K and solid state spectrum in a KBr pellet at room temperature (298 K).

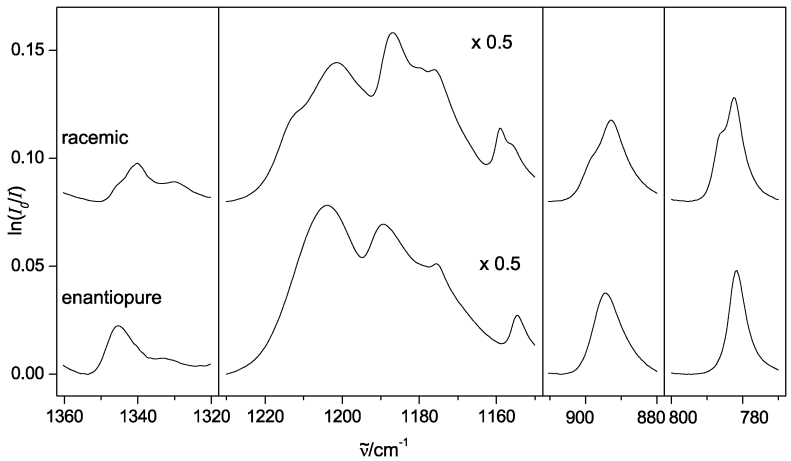

Fig. 13 ATR spectra of crystalline racemic and enantiopure methyl mandelate in selected spectral regions where differences were observed (4 × 50 averaged scans).

high frequency slopes of most racemate peaks in Fig. 13. We have recorded equivalent spectra of the compounds embedded in KBr pellets (not shown). They show similar spectral trends, but are significantly more diffuse.

In Fig. 14, the far infrared spectra of racemic and enantiopure methyl mandelate are compared to each other in the range of 30–470 cm^{-1}. One can see that the relative differences between the two crystal forms are substantially more pronounced in this spectral range, as expected for the associated large amplitude collective motions. Particularly notable are the intensity gain and sharpening at 220 cm^{-1}, the shifts at 60 and 170 cm^{-1} as well as the appearance of a new peak at 340 cm^{-1} upon including the mirror image molecule into the crystal.

3.5 X-ray structures

Within the scope of this work three single crystal X-ray structure determinations were carried out. Crystals were first obtained for the *S*-enantiomer, which was crystallized by cooling of an oversaturated aqueous solution. Structure solution and refinement was straightforward and four independent molecules pack in the asymmetric unit in monoclinic space group $P2_1$. Large single crystals of the *S*-enantiomer can also

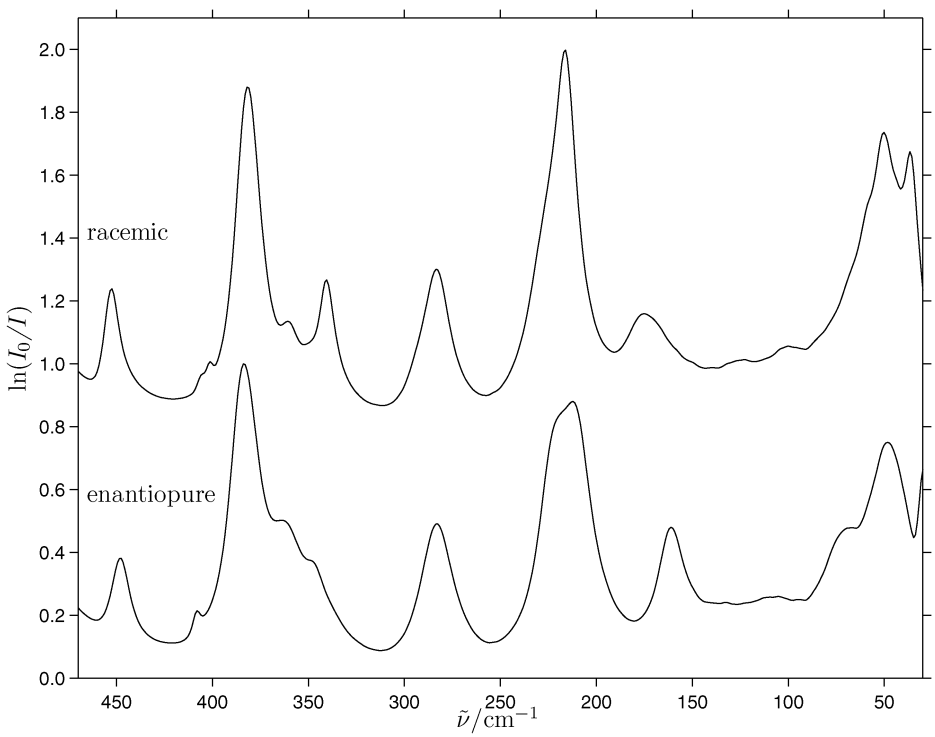

Fig. 14 Far infrared diamond ATR spectra of racemic and enantiopure methyl mandelate crystals between 30 and 470 cm^{-1}. Note that on a wavenumber ratio scale, the chirality recognition effects are substantial and reflect the long range differences experienced by lattice vibrations.

Table 5 Crystal structure and refinement data for three methyl mandelate structures (*S*, racemic, *RRRS*). Full details can be found in the CIF-files of the supplementary information

Formula	$C_9H_{10}O_3$		
Formula weight	166.17		
Crystal system	Monoclinic	Triclinic	Monoclinic
Space group, Z	$P2_1$(No. 4), 8	$P\bar{1}$ (No. 2), 8	$P2_1$ (No. 4), 8
a/Å	7.8825(4)	7.8576(2)	11.0955(9)
b/Å	20.1054(11)	11.0894(4)	7.8081(5)
c/Å	10.7516(5)	20.0502(7)	19.7538(16)
α (°)	90	103.782(2)	90
β (°)	91.033(3)	98.959(2)	104.259(5)
γ (°)	90	92.247(2)	90
V/Å^3	1703.65(15)	1670.78(10)	1658.6(2)
T/K	100	100	100
Tot., Uniq. Data, R(int)	22455, 5847, 0.050	26447, 5946, 0.034	27403, 5618, 0.036
Observed data*	5259	4717	4538
R [%], $wR2$ [%], S	4.12, 4.88, 2.26	4.60, 4.91, 3.51	2.94, 2.64, 1.99
Weighting scheme	$w = 1/\sigma^2(F_o)$	$w = 1/\sigma^2(F_o)$	$w = 1/\sigma^2(F_o)$
Flack x	0.10(16)	—	0.10(15)
$\Delta\rho_{min}$, $\Delta\rho_{max}$/[e Å^{-3}]	−0.27, 0.24	−0.25, 0.63	−0.17, 0.18

$R(\text{int})(F^2) = \sum|F_o^2 - F_o^2(mean)|/\sum F_o^2$, $wR2 = \{\sum[w(F_o^2 - F_c^2)^2]/\sum[w(F_c^2)]\}^{1/2}$, $R = \sum||F_o| - |F_c||/\sum|F_o|$, $S = \{\sum||F_o| - k|F_c||^2/(n_o - m_{var})\}^{1/2}$, *Refinement on F with $F > 3\sigma(F)$.

be grown by sublimation. Attempts to obtain single crystals by sublimation for the racemate starting from a racemic mixture were unsuccessful. However, these attempts afforded a *RRRS*-form, which again crystallizes in the chiral monoclinic space group $P2_1$. Crystal quality of this *RRRS*-form was poor, but after several crystallization attempts finally a small untwinned specimen was obtained. The formation of non-racemic, non-enantiopure crystals from racemic mixtures is rather rare.[3,85] Although several further attempts were carried out repeating sublimation experiments with *R*/*S* mixtures of different composition, a racemic crystal of *R*- and *S*-form was only obtained from a solution of the racemate in toluene. Surprisingly, the same *RRRS* (or *SSSR*) alternation in the infinite hydrogen bonded chains is again observed in the racemic crystal; molecules crystallize in the triclinic space group $P\bar{1}$. Details on the crystal structures can be found in Table 5. For further information on the X-ray structures we refer to the CIF-files of the supplementary material provided with this manuscript.†

The three crystal structures for the *S*, *RRRS* and *RS* forms may be analyzed with respect to three types of bonding, which dominate along the three space dimensions. In the dimension which we denote H, there are infinite zig-zag chains or ribbons of bifurcated hydrogen bonds which the OH group undergoes with the C=O and O–H groups of the neighboring molecule. This motif does not occur in the dimers we have discussed but it is known from methyl lactate trimers.[11] In a more or less orthogonal dimension, which we denote A, aromatic rings of neighboring chains undergo π–π interactions by interlocking with each other. The resulting layers of alternating hydrogen bond and aromatic interaction zones are stapled on top of each other *via* van der Waals interactions between methylester groups and aromatic rings along a dimension which we call W. This general HAW-pattern is common to all structures. In particular, the hydrogen bond connectivity is always the same, as illustrated for the *RRRS*-form in Fig. 15 (HW projection). The major difference is found in the details of the aromatic ring zone (A dimension). In the enantiopure compound, the aromatic rings alternate along the zig-zag chain, pointing up in the zig-row and down in the zag-row. Therefore, the hydrogen-bonded chains can be stapled efficiently with a large contact area. In the 50%ee case, every fourth phenyl group points in the other direction. This leads to a particular interlock of the *RRRS* chain staples (see Fig. 15). The racemic (0%ee) form actually consists of alternating layers of *RSSS* and *SRRR* structures, leading to 8 molecules in the unit cell. The phase diagram of methyl mandelate is thus expected to have three dystectic points, namely *SRRR*, *RS*, *RSSS*.

We note that the far IR spectrum of a sample of *RRRS* composition is similar to that of the racemic crystals, with some elements of the enantiopure solid state spectra. It cannot be represented by a linear superposition of the two others, thus supporting the existence of a specific *RRRS* crystal structure.

3.6 Bulk vapor pressures

Although the spectra of the crystalline methyl mandelate in a KBr pellet and in ATR mode show only subtle differences between the enantiopure and racemic sample and their hydrogen bond pattern is the same, their vapor pressure is significantly different. Using quadrupole mass spectrometry, a 1.20 ± 0.10 times higher vapor pressure of the enantiopure sample compared to the racemic mixture was consistently observed at 293.0 ± 0.5 K, based on the mass peaks 79 and 107 (Fig. S6†).

This vapor pressure difference must be attributed to intermolecular diastereoisomerism, possibly related to different packings of the aromatic groups. In a way, this is the OH···OH version of the OH···OC-mediated chirality recognition phenomenon in the isolated dimer.

Samples with *RRRS* composition were also investigated. The vapor pressure of the *RRRS* sample is close to that expected for a eutectic *R*/*RS* composition,[86,87] *i.e.* another 10–20% higher than the enantiopure vapor pressure. The complexity of the phase diagram requires a more detailed study in order to draw specific conclusions from this value.

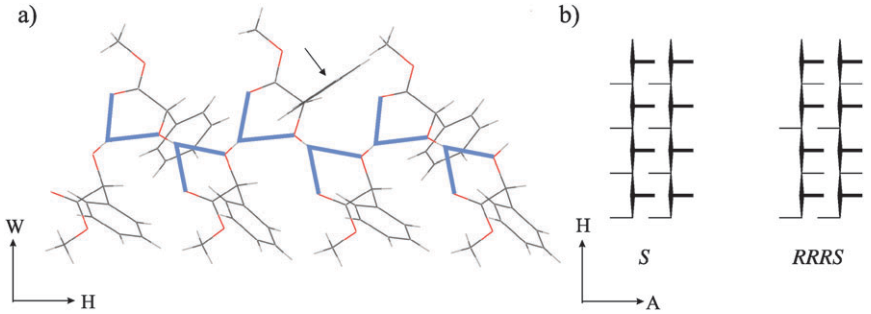

Fig. 15 (a) Chain segment from the crystal structure of the *RRRS* crystal. The benzene ring marked with an arrow is pointing towards the observer. Bifurcated hydrogen bonds from the OH group to the neighboring OH group and the neighboring C═O group are marked with thick lines. (b) Schematic view of the crystal structures in the plane defined by hydrogen bonds (H) and aromatic interactions (A). The vertical line symbolizes a hydrogen bond strand, as shown in part (a). The horizontal lines symbolize aromatic side groups.

4 Conclusions

Methyl mandelate is an interesting homolog of the stereoselectively aggregating methyl lactate.[11] It comes with an additional functionality which competes in many different ways with the existing intermolecular contacts in an α-hydroxy ester, namely the aromatic π system. This may act as a weak acceptor towards dangling OH groups and it can undergo dispersive π–π and CH–π interactions at different orientations with neighboring aromatic units.[35]

We were able to show that the most stable homodimer structures involve two C═O···HO hydrogen bonds in a floppy 8-ring system, which is constrained by π–π interactions between the phenyl rings. The spectra indicate that a T-shaped, rather than a slipped parallel arrangement of the phenyl rings is preferred.

If one of the mandelate units in the dimer is replaced by its mirror image, this synergy between hydrogen bond and aromatic interactions is no longer possible. The global minimum structure appears to be one in which π–π interactions are enabled at the price of a broken hydrogen bond. The dangling hydrogen bond partners build secondary interactions with the backbone of the neighboring molecule. Even dimer structures with no intermolecular hydrogen bond are competitive and may be formed in the early stage of a supersonic jet expansion.

Methyl mandelate is thus an example for serious competition between aromatic interactions and hydrogen bonding. This is only possible because the molecule itself contains an intramolecular hydrogen bond, which attenuates the energy gain associated with the formation of an intermolecular hydrogen bridge. Such subtle balances between intra- and intermolecular hydrogen bonds are at the heart of biomolecular structure and function, and mandelates are gas phase model systems which describe this competition.

The infrared spectra of methyl mandelate and its clusters were obtained in different ways. IR/UV double resonance has the advantage of conformational and size selectivity and was able to discriminate two different heterochiral dimers. FTIR spectroscopy allows for a direct comparison with non-aromatic homologs to work out the role which π interactions play in molecular recognition.

While MP2 calculations turned out to be helpful for the approximate identification of global dimer minimum structures, their spectra were predicted by the more economic DFT-D method, thus emphasizing the value of this semiempirical extension of density functional theory. Uncorrected "dispersion-blind" semi-local or hybrid functionals are not useful for the analysis of mandelate aggregation. Because the relatively high accuracy of DFT-D has meanwhile been demonstrated many times (and once again in this study), in future work one should change the computational strategy and search the conformational space with the very cheap DFT-D method and perform the single-point energy computations of the relative energies (populations) by complete basis set extrapolation techniques and higher-level correlation methods of either wavefunction (*e.g.* with third-order terms[88]) or DFT type (*e.g.* double hybrid functionals[89]). If higher accuracy is necessary in the spectral simulations, the rather expensive computations of harmonic (and eventually anharmonic) frequencies could also be performed (assuming steadily increasing computer hardware capabilities) at the dispersion-corrected hybrid functional level.

Beyond the characterization of mandelate dimers, this study provides evidence for the absence of tetramers with isolated C═O···HO hydrogen bonds, which are so prominent in lactates.[10] It demonstrates that the internal hydrogen bond of the monomers can be partially preserved by depositing them as a glassy layer on a cold surface. At higher temperatures and in the crystal, the intramolecular hydrogen bonds are broken in favor of extended chains, held together by cooperative OH···OH interactions which are augmented with bifurcation to C═O. These infinite chain arrangements also show chirality recognition, which may be detected as a significant vapor pressure difference between the crystals of the racemic mixture and the enantiopure crystal and as slight differences in the IR spectra. Crystallographic analysis indicates that these differences are again directly related to aromatic ring interactions, and not so much to the hydrogen bonds themselves. The pattern of the latter is reminiscent of that in cyclic lactate trimers, whereas it is not found in the most stable dimers.

In the future, it will be attractive to extend our studies to mandelic acid, which is of direct relevance in racemate separations and involves an additional strong hydrogen bond contact. Stereoselective effects on reactivity have been observed in the formation of polyesters from mandelic acid.[90] One should

however note that intermolecular interactions in carboxylic acids are dominated by the stiff double hydrogen bonds in the dimer.[91] This stiffness pulls the stereocenters away from each other, making chirality recognition in dimers more difficult to detect. The ester group in methyl mandelate blocks this strong interaction and allows for substantial chirality recognition effects already at the level of molecular pairs.

Acknowledgements

The present work was supported by the Fonds der Chemischen Industrie and by the DFG research training group 782 (www.pcgg.de). It has profited from DAAD/GRICES-funded student exchange of A. Borba and M. Albrecht. A. Borba thanks the Portuguese Science Foundation (FCT) and the grant ref. SFRH/BD/21543/2005. K. LeBarbu-Debus thanks the DI (Orsay) for the allotment of computational resources. A. Zehnacker-Rentien thanks the CLUPS (Orsay) for making the IR-UV measurements possible. We thank C. Rice for help and discussions. K. Lossie and S. Polk have contributed to this study during their undergraduate practical course. B. Dittrich thanks the DFG for an Emmy Noether fellowship (DFG DI/921/3-1).

References

1 A. Zehnacker and M. A. Suhm, Chirality recognition between neutral molecules in the gas phase, *Angew. Chem., Int. Ed.*, 2008, **47**, 6970–6992.
2 J. S. Chickos and D. G. Hesse, An experimental test of the double solubility rule, *Struct. Chem.*, 1991, **2**, 33–40.
3 J. Jacques, A. Collet and S. H. Wilen, *Enantiomers, Racemates, and Resolutions*, Wiley, New York, 1981.
4 A. Fischer and V. M. Profir, A metastable modification of (*RS*)-mandelic acid, *Acta Crystallogr., Sect. E: Struct. Rep. Online*, 2003, **59**, o1113–o1116.
5 S. B. Tsogoeva, S. Wei, M. Freund and M. Mauksch, Generation of highly enantioenriched crystalline products in reversible asymmetric reactions with racemic or achiral catalysts, *Angew. Chem., Int. Ed.*, 2009, **48**, 590–594.
6 M. S. Taylor and E. N. Jacobsen, Asymmetric catalysis by chiral hydrogen-bond donors, *Angew. Chem., Int. Ed.*, 2006, **45**, 1520–1543.
7 P. Yang, R. Xu, S. C. Nanita and R. G. Cooks, Thermal formation of homochiral serine clusters and implications for the origin of homochirality, *J. Am. Chem. Soc.*, 2006, **128**, 17074–17086.
8 M. Speranza, Enantioselectivity in gas-phase ionmolecule reactions, *Int. J. Mass Spectrom.*, 2004, **232**, 277–317.
9 W. A. Tao and R. G. Cooks, Chiral analysis by MS, *Analyt. Chem.*, 2003, **75**, 25A–31A.
10 T. B. Adler, N. Borho, M. Reiher and M. A. Suhm, Chirality-induced switch in hydrogen bond topology: Tetrameric methyl lactate clusters in the gas phase, *Angew. Chem., Int. Ed.*, 2006, **45**, 3440–3445.
11 N. Borho and M. A. Suhm, Self-organization of lactates in the gas phase, *Org. Biomol. Chem.*, 2003, **1**, 4351–4358.
12 M. Fárník, M. Weimann, C. Steinbach, U. Buck, N. Borho, T. B. Adler and M. A. Suhm, Size-selected methyl lactate clusters: fragmentation and spectroscopic fingerprints of chiral recognition, *Phys. Chem. Chem. Phys.*, 2006, **8**, 1148–1158.
13 K. Le Barbu, F. Lahmani and A. Zehnacker-Rentien, Formation of hydrogen-bonded structures in jet-cooled complexes of a chiral chromophore studied by IR/UV double resonance spectroscopy: diastereoisomeric complexes of (±)-2-naphthyl-1-ethanol with (±)-2-amino-1-propanol, *J. Phys. Chem. A*, 2002, **106**, 6271–6278.
14 N. Seurre, J. Sepioł, K. Le Barbu-Debus, F. Lahmani and A. Zehnacker-Rentien, The role of chirality in the competition between inter and intramolecular hydrogen bonds: jet-cooled van der Waals complexes of (±)2-naphthyl-1-ethanol with (±)1-amino-2-propanol and (±)2-amino-1-butanol, *Phys. Chem. Chem. Phys.*, 2004, **6**, 2867–2877.
15 N. Seurre, K. Le Barbu-Debus, F. Lahmani, A. Zehnacker-Rentien and J. Sepiol, Structural study of hydrogen-bonded complexes between 2-aminoethanol derivatives and a chiral aromatic alcohol, *J. Mol. Struct.*, 2004, **692**, 127–137.
16 N. Seurre, K. Le Barbu-Debus, F. Lahmani, A. Zehnacker, N. Borho and M. A. Suhm, Chiral recognition between lactic acid derivatives and an aromatic alcohol in a supersonic expansion: electronic and vibrational spectroscopy, *Phys. Chem. Chem. Phys.*, 2006, **8**, 1007–1016.
17 M. Albrecht, C. A. Rice and M. A. Suhm, Elementary peptide motifs in the gas phase: FTIR aggregation study of formamide, acetamide, *N*-methylformamide and *N*-methylacetamide, *J. Phys. Chem. A*, 2008, **112**, 7530–7542.
18 E. C. Lee, D. Kim, P. Jurečka, P. Tarakeshwar, P. Hobza and K. S. Kim, Understanding of assembly phenomena by aromatic–aromatic interactions: Benzene dimer and the substituted systems, *J. Phys. Chem. A*, 2007, **111**, 3446–3457.
19 K. Le Barbu-Debus, M. Broquier, A. Mahjoub and A. Zehnacker-Rentien, Chiral recognition in jet-cooled complexes of (1*R*,2*S*)-(+)-cis-1-amino-2- indanol and methyl lactate: on the importance of the CH···π interaction, *Phys. Chem. Chem. Phys.*, 2009, **11**, 7589–7598.
20 G. D. Yadav, A. D. Sajgure and S. B. Dhoot, Insight into microwave irradiation and enzyme catalysis in enantioselective resolution of RS-(±)-methyl mandelate, *J. Chem. Technol. Biotechnol.*, 2008, **83**, 1145–1153.
21 N. Mori, Y. Tanaka and Y. Tsuzuki, Intramolecular hydrogen bonds. VII. Methyl mandelates and related compounds, *Bull. Chem. Soc. Jpn.*, 1966, **39**, 1490–1495.
22 N. Mori, Y. Asano, T. Irie and Y. Tsuzuki, Intramolecular hydrogen bonds. XIII. The preferable conformation of α-hydroxycarboxylic and *o*-hydroxybenzoic Acids, *Bull. Chem. Soc. Jpn.*, 1969, **42**, 482–487.
23 R. J. Piffath and S. Sass, An infrared study of the methyl esters of phenylglycolic acids and related compounds, *Appl. Spectrosc.*, 1972, **26**, 92–95.
24 K. Le Barbu-Debus, M. Broquier, A. Mahjoub and A. Zehnacker-Rentien, Chiral recognition between α-hydroxylesters: A double-resonance IR/UV study of the complexes of methyl mandelate with methyl glycolate and methyl lactate, *J. Phys. Chem. A*, 2008, **112**, 9731–9741.
25 N. Borho and M. A. Suhm, Tailor-made aggregates of α-hydroxy esters in supersonic jets, *Phys. Chem. Chem. Phys.*, 2004, **6**, 2885–2890.
26 A. Borba, A. Gómez-Zavaglia, L. Lapinski and R. Fausto, Matrix isolation FTIR spectroscopic and theoretical study of methyl lactate, *Vib. Spectrosc.*, 2004, **36**, 79–88.
27 P. Ottaviani, B. Velino and W. Caminati, Jet cooled rotational spectrum of methyl lactate, *Chem. Phys. Lett.*, 2006, **428**, 236–240.
28 N. Borho and Y. Xu, Rotational spectrum of a chiral α-hydroxy-ester: conformation stability and internal rotation barrier heights of methyl lactate, *Phys. Chem. Chem. Phys.*, 2007, **9**, 1324–1328.
29 S. Aparicio, Computational study on the properties and structure of methyl lactate, *J. Phys. Chem. A*, 2007, **111**, 4671–4683.
30 M. Losada and Y. Xu, Chirality transfer through hydrogen-bonding: Experimental and *ab initio* analyses of vibrational circular dichroism spectra of methyl lactate in water, *Phys. Chem. Chem. Phys.*, 2007, **9**, 3127–3135.
31 A. Borba, M. Albrecht, A. Gómez-Zavaglia, L. Lapinski, M. J. Novak, M. A. Suhm and R. Fausto, Dimer formation in nicotinamide and picolinamide in the gas and condensed phases probed by infrared spectroscopy, *Phys. Chem. Chem. Phys.*, 2008, **10**, 7010–7021.
32 I. Alkorta, Ó. Picazo and J. Elguero, Theoretical studies on chiral discrimination, *Curr. Org. Chem.*, 2006, **10**, 695–714.
33 J. Antony and S. Grimme, Density functional theory including dispersion correction for intermolecular interactions in a large benchmark set of biologically relevant molecules, *Phys. Chem. Chem. Phys.*, 2006, **8**, 5287–5293.
34 S. Grimme, J. Antony, T. Schwabe and C. Mück-Lichtenfeld, Density functional theory with dispersion corrections for

supramolecular structures, aggregates and complexes of (bio)-organic molecules, *Org. Biomol. Chem.*, 2007, **5**, 741–758.
35 S. Grimme, Do special noncovalent π–π stacking interactions really exist?, *Angew. Chem., Int. Ed.*, 2008, **47**, 3430–3434.
36 I. D. Reva, S. G. Stepanian, L. Adamowicz and R. Fausto, Combined FTIR matrix isolation and *Ab initio* studies of pyruvic acid: Proof for existence of the second conformer, *J. Phys. Chem. A*, 2001, **105**, 4773–4780.
37 A. Borba, A. Gómez-Zavaglia, P. N. N. L. Simões and R. Fausto, Matrix-isolation FT-IR spectra and theoretical study of dimethyl sulfate, *Spectrochim. Acta, Part A*, 2005, **61**, 1461–1470.
38 APEX2, SAINT and SADABS, Bruker AXS Inc. Madison, Wisconsin, USA, 2008.
39 G. M. Sheldrick, A short history of SHELX, *Acta Crystallogr., Sect. A: Found. Crystallogr.*, 2008, **64**, 112–122.
40 B. Dittrich, C. B. Hübschle, P. Luger and M. A. Spackman, Introduction and validation of an invariom database for amino-acid, peptide and protein molecules, *ActaCrystallogr., Sect. D: Biol. Crystallogr.*, 2006, **62**, 1325–1335.
41 T. Koritsanszky, T. Richer, P. Macchi, A. Volkov, C. Gatti, S. Howard, P. R. Mallinson, L. Farrugia, Z. Su and N. K. Hansen, *XD-a computer program package for multipole refinement and topological analysis of electron densities from diffraction data*, Freie Universität Berlin, 2003.
42 N. K. Hansen and P. Coppens, Testing aspherical atom refinements on small-molecule data sets, *Acta Crystallogr., Sect. A: Cryst. Phys., Diffr., Theor. Gen. Crystallogr.*, 1978, **34**, 909–921.
43 B. Dittrich, M. Strumpel, M. Schäfer, M. A. Spackman and T. Koritsanszky, Invarioms for improved absolute structure determination of light-atom crystal structures, *Acta Crystallogr., Sect. A: Found. Crystallogr.*, 2006, **62**, 217–223.
44 H. D. Flack, On enantiomorph-polarity estimation, *Acta Crystallogr., Sect. A: Found. Crystallogr.*, 1983, **39**, 876–881.
45 R. W. W. Hooft, L. H. Straver and A. L. Spek, Determination of absolute structure using Bayesian statistics on Bijvoet differences, *J. Appl. Crystallogr.*, 2008, **41**, 96–103.
46 H. D. Flack and G. Bernardinelli, Reporting and evaluating absolute-structure and absolute-configuration determinations, *J. Appl. Crystallogr.*, 2000, **33**, 1143–1148.
47 C. Cézard, C. A. Rice and M. A. Suhm, OH-stretching redshifts in bulky hydrogen-bonded alcohols: Jet spectroscopy and modeling, *J. Phys. Chem. A*, 2006, **110**, 9839–9848.
48 M. Kameyama, N. Kamigata and M. Kobayashi, Asymmetric radical reaction in the coordination sphere. 2. asymmetric addition of alkane- and arenesulfonyl chlorides to olefins catalyzed by a Ruthenium(II)-Phosphine complex with chiral ligands, *J. Org. Chem.*, 1987, **52**, 3312–3316.
49 M. Selva and P. Tundo, Highly chemoselective methylation and esterification reactions with dimethyl carbonate in the presence of NaY faujasite. The case of mercaptophenols, mercaptobenzoic acids and carboxylic acids bearing OH substituents, *J. Org. Chem.*, 2006, **71**, 1464–1470.
50 A. Mahjoub, A. Chakraborty, V. Lepere, K. Le Barbu-Debus, N. Guchhait and A. Zehnacker, Chirality-dependent hydrogen bond direction in jet-cooled (*S*)-1,2,3,4-tetrahydro-3-isoquinoline methanol (THIQM): IR-ion dip vibrational spectroscopy of the neutral and the ion, *Phys. Chem. Chem. Phys.*, 2009, **11**, 5160–5169.
51 K. Nasirzadeh, R. Neueder and W. Kunz, Vapor pressure determination of the aliphatic C_5 to C_8 1-Alcohols, *J. Chem. Eng. Data*, 2006, **51**, 7–10.
52 A. Rose, B. Papahronis and E. Williams, Experimental measurement of vapor-liquid equilibria for octanol-decanol and decanol-dodecanol binaries, *Chem. Eng. Data Ser.*, 1958, **3**, 216–219.
53 M. J. Frisch, G. W. Trucks, H. B. Schlegel, G. E. Scuseria, M. A. Robb, J. R. Cheeseman, J. A. Montgomery, Jr., T. Vreven, K. N. Kudin, J. C. Burant, J. M. Millam, S. S. Iyengar, J. Tomasi, V. Barone, B. Mennucci, M. Cossi, G. Scalmani, N. Rega, G. A. Petersson, H. Nakatsuji, M. Hada, M. Ehara, K. Toyota, R. Fukuda, J. Hasegawa, M. Ishida, T. Nakajima, Y. Honda, O. Kitao, H. Nakai, M. Klene, X. Li, J. E. Knox, H. P. Hratchian, J. B. Cross, C. Adamo, J. Jaramillo, R. Gomperts, R. E. Stratmann, O. Yazyev, A. J. Austin, R. Cammi, C. Pomelli, J. W. Ochterski, P. Y. Ayala, K. Morokuma, G. A. Voth, P. Salvador, J. J. Dannenberg, V. G. Zakrzewski, S. Dapprich, A. D. Daniels, M. C. Strain, O. Farkas, D. K. Malick, A. D. Rabuck, K. Raghavachari, J. B. Foresman, J. V. Ortiz, Q. Cui, A. G. Baboul, S. Clifford, J. Cioslowski, B. B. Stefanov, G. Liu, A. Liashenko, P. Piskorz, I. Komaromi, R. L. Martin, D. J. Fox, T. Keith, M. A. Al-Laham, C. Y. Peng, A. Nanayakkara, M. Challacombe, P. M. W. Gill, B. Johnson, W. Chen, M. W. Wong, C. Gonzalez and J. A. Pople, *GAUSSIAN 03, Revisions B.04 and C.02.*, Gaussian Inc., Pittsburgh PA, 2003.
54 S. Grimme, Semiempirical GGA-type density functional constructed with a long-range dispersion correction, *J. Comput. Chem.*, 2006, **27**, 1787–1799.
55 K. Eichkorn, F. Weigend, O. Treutler and R. Ahlrichs, Auxiliary basis sets for main row atoms and transition metals and their use to approximate Coulomb potentials, *Theor. Chem. Acc.*, 1997, **97**, 119–124.
56 F. Weigend and R. Ahlrichs, Balanced basis sets of split valence, triple zeta valence and quadruple zeta valence quality for H to Rn: Design and assessment of accuracy, *Phys. Chem. Chem. Phys.*, 2005, **7**, 3297–3305.
57 TURBOMOLE, version 5.9: Ahlrichs *et al.*, Universität Karlsruhe 2007. See http://www.turbomole.com.
58 K. Le Barbu, V. Brenner, P. Millie, F. Lahmani and A. Zehnacker-Rentien, An experimental and theoretical study of jet-cooled complexes of chiral molecules: The role of dispersive forces in chiral discrimination, *J. Phys. Chem. A*, 1998, **102**, 128–137.
59 J. Neugebauer, M. Reiher, C. Kind and B. A. Hess, Quantum chemical calculation of vibrational spectra of large molecules – Raman and IR spectra for Buckminsterfullerene, *J. Comput. Chem.*, 2002, **23**, 895–910.
60 F. Lahmani, C. Lardeux-Dedonder and A. Zehnacker, Spectroscopy and dynamics of benzonitrile-enzene complexes in a supersonic free-jet, *Laser Chem.*, 1989, **10**, 41–50.
61 A. Zehnacker, F. Lahmani, E. Bréhéret, J. P. Desvergne, H. Bouas-Laurent, A. Germain, V. Brenner and P. Millié, Laser induced fluorescence of jet-cooled non-conjugated bichromophores: bis-phenoxymethane and bis-2,6-dimethylphenoxymethane, *Chem. Phys.*, 1996, **208**, 243–257.
62 F. Lahmani, C. Lardeux-Dedonder, D. Solgadi and A. Zehnacker, Molecular jet study and calculations of the vibronic structure of the aniline-benzene van der Waals complex, *Chem. Phys.*, 1988, **120**, 215–223.
63 T. Kobayashi, K. Honma, O. Kajimoto and S. Tsuchiya, Benzonitrile and its van der Waals complexes studied in a free jet. I. The LIF spectra and the structure, *J. Chem. Phys.*, 1987, **86**, 1111–1117.
64 K. O. Bornsen, H. L. Selzle and E. W. Schlag, The Interactions in the benzene dimer in a supersonic jet-study of the S_1 level with isotopic labeling, *Z. Naturforsch. A-J. Phys. Sci.*, 1984, **39**, 1255–1258.
65 M. Sakai, S. Ishiuchi and M. Fujii, Picosecond time-resolved nonresonant ionization detected IR spectroscopy on 7-azaindole dimer, *Eur. Phys. J. D*, 2002, **20**, 399–402.
66 R. W. Larsen, P. Zielke and M. A. Suhm, Hydrogen-bonded OH stretching modes of methanol clusters: A combined IR and Raman isotopomer study, *J. Chem. Phys.*, 2007, **126**, 194307.
67 S. Kristyán and P. Pulay, Can (semi)local density functional theory account for the London dispersion forces, *Chem. Phys. Lett.*, 1994, **229**, 175–180.
68 P. Hobza, J. Sponer and T. Reschel, Density functional theory and molecular clusters, *J. Comput. Chem.*, 1995, **16**, 1315–1325.
69 J. Antony and S. Grimme, Is spin-component scaled second-order Møller–Plesset perturbation theory an appropriate method for the study of noncovalent interactions in molecules?, *J. Phys. Chem. A*, 2007, **111**, 4862–4868.
70 J. G. Hill, J. A. Platts and H.-J. Werner, Calculation of intermolecular interactions in the benzene dimer using coupled-cluster and local electron correlation methods, *Phys. Chem. Chem. Phys.*, 2006, **8**, 4072–4078.
71 M. O. Sinnokrot and C. D. Sherrill, Highly accurate coupled cluster potential energy curves for the benzene dimer: Sandwich, T-shaped and parallel-displaced configurations, *J. Phys. Chem. A*, 2004, **108**, 10200–10207.
72 C. D. Sherrill, T. Takatani and E. G. Hohenstein, An assessment of theoretical methods for nonbonded interactions: Comparison to complete basis set limit coupled-cluster potential energy curves for

the benzene dimer, the methane dimer, benzene-methane and benzene-H_2S, *J. Phys. Chem. A*, 2009, **113**, 10146–10159.
73 H. Krause, B. Ernstberger and H. J. Neusser, Binding energies of small benzene clusters, *Chem. Phys. Lett.*, 1991, **184**, 411–417.
74 J. R. Grover, E. A. Walters and E. T. Hui, Dissociation energies of the benzene dimer and dimer cation, *J. Phys. Chem.*, 1987, **91**, 3233–3237.
75 Nicole Borho, *PhD thesis*, Universität Göttingen, 2004.
76 S. Grimme, J. Antony, T. Schwabe and C. Mück-Lichtenfeld, Density functional theory with dispersion corrections for supramolecular structures, aggregates and complexes of (bio)organic molecules, *Org. Biomol. Chem.*, 2007, **5**, 741–758.
77 S. Grimme and C. Mück-Lichtenfeld, Calculation of conformational energies and optical rotation of the most simple chiral alkane, *Chirality*, 2008, **20**, 1009–1015.
78 S. Grimme, C. Mück-Lichtenfeld and J. Antony, Noncovalent interactions between graphene sheets and in multishell (hyper)-fullerenes, *J. Phys. Chem. C*, 2007, **111**, 11199–11207.
79 C. Mück-Lichtenfeld and S. Grimme, Structure and binding energies of the porphine dimer, *Mol. Phys.*, 2007, **105**, 2793–2798.
80 T. Häber, K. Seefeld, G. Engler, S. Grimme and K. Kleinermanns, IR/UV spectra and quantum chemical calculations of TrpSer: Stacking interactions between backbone and indole side-chain, *Phys. Chem. Chem. Phys.*, 2008, **10**, 2844–2851.
81 C. Maerker, P. v. R. Schleyer, K. R. Liedl, T. K. Ha, M. Quack and M. A. Suhm, A critical analysis of electronic density functionals for structural, energetic, dynamic and magnetic properties of hydrogen fluoride clusters, *J. Comput. Chem.*, 1997, **18**, 1695–1719.
82 M. Mons, F. Piuzzi, I. Dimicoli, A. Zehnacker and F. Lahmani, Binding energy of hydrogen-bonded complexes of the chiral molecule 1-phenylethanol, as studied by 2C-R2PI: comparison between diastereoisomeric complexes with butan-2-ol and the singly hydrated complex, *Phys. Chem. Chem. Phys.*, 2000, **2**, 5065–5070.
83 K. Le Barbu, F. Lahmani, M. Mons, M. Broquier and A. Zehnacker, IR–UV investigation of the structure of the 1-phenylethanol chromophore and its hydrated complexes, *Phys. Chem. Chem. Phys.*, 2001, **3**, 4684–4688.
84 U. Erlekam, M. Frankowski, G. von Helden and G. Meijer, Cold collisions catalyse conformational conversion, *Phys. Chem. Chem. Phys.*, 2007, **9**, 3786–3789.
85 H. E. Gallis, P. J. van Ekeren, J. C. van Miltenburg and H. A. J. Oonk, Mixtures of *d*- and *l*-carvone IV. Transformation from a solid solution to a racemic compound, *Thermochim. Acta*, 1999, **326**, 83–90.
86 M. Albrecht, V. A. Soloshonok, L. Schrader, M. Yasumoto and M. A. Suhm, Chirality-dependent sublimation of α-(trifluoromethyl)-lactic acid: Relative vapor pressures of racemic, eutectic and enantiomerically pure forms and vibrational spectroscopy of isolated (*SS*) and (*SR*) dimers, *J. Fluorine Chem.*, 2010, **131**, 495–504.
87 M. Farina and G. Di Silvestro, Solid-liquid–vapor equilibria of chiral compounds, *Mol. Cryst. Liq. Cryst. Inc. Nonlin. Opt.*, 1988, **161**, 177–198.
88 M. Pitonak, P. Neograd, J. Cerny, S. Grimme and P. Hobza, Scaled MP3 non-covalent interaction energies agree closely with accurate CCSD(T) benchmark data, *ChemPhysChem*, 2009, **10**, 282–289.
89 S. Grimme and T. Schwabe, Theoretical thermodynamics for large molecules: Walking the thin line between accuracy and computational cost, *Acc. Chem. Res.*, 2008, **41**, 569–579.
90 K. J. Whitesell and J. A. Pojman, Homochiral and heterochiral polyesters: Polymers derived from mandelic acid, *Chem. Mater.*, 1990, **2**, 248–254.
91 P. Zielke and M. A. Suhm, Raman jet spectroscopy of formic acid dimers: low frequency vibrational dynamics and beyond, *Phys. Chem. Chem. Phys.*, 2007, **9**, 4528–4534.